

Please check the marked (■) text passages carefully.

High Temperature Solid Oxide Electrolysis – Technology and Modeling

Marius Mueller*, Markus Klinsmann, Ulrich Sauter, Jean-Claude Njodzefon, and André Weber

DOI: 10.1002/cite.202300137

This is an open access article under the terms of the Creative Commons Attribution-NonCommercial-NoDerivs License, which permits use and distribution in any medium, provided the original work is properly cited, the use is non-commercial and no modifications or adaptations are made.

In the global quest to renounce from fossil fuels, a large demand for the renewable production of hydrogen via water electrolysis exists. In this context, the solid oxide electrolyzer (SOE) is an interesting technology due to its high efficiency resulting from elevated operating temperatures of up to 900 °C. Physical modeling plays a vital role in the development of SOEs, as it lowers experimental costs and provides insight where measurements reach limits. A main challenge for modeling SOEs is the multitude of physical effects, occurring and interacting on various spatial and temporal scales. This requires assumptions and simplifications, particularly when increasing scope and dimensions of a model. In this review, we discuss the different approaches currently available in literature.

Keywords: Electrolysis, Modeling, Multiphysics, Solid oxide cell

Received: July 31, 2023; *accepted:* December 05, 2023

1 Introduction

In wake of climate change, substituting fossil fuels with renewables has become a common goal. One challenge faced by this transformation is the fluctuating nature of wind and solar energies which leads to periods where power demand is either not met or exceeded. To bridge timespans where power generation from renewable sources is low, it is necessary to effectively store the surplus energy and feed it into the power grid when needed. Converting electrical to chemical energy in form of hydrogen or its derivatives via the electrolysis of water is a potent way to address this challenge. The produced hydrogen can be stored in the liquid state, compressed in storage tanks or underground caverns [1] or mixed into the natural gas network [2]. Further chemical storage media include ammonia, methanol, liquid hydrogen carriers, dimethyl ether and other synthetic fuels [3].

Next to energy conversion and storage, chemicals have to be produced in a renewable way. Many chemical substances are nowadays produced from natural gas or oil, which must be substituted by renewable hydrogen and syngas.

Currently, while most of the global hydrogen is won through CO₂-emitting steam reforming, only 5% is produced from renewable resources including water electrolysis [4]. State of the art electrolysis technologies include the traditional alkaline electrolysis (AEL). Being the most mature electrolysis technology, longest lifetimes have been demonstrated with it. Followed in maturity and market availability is the polymer membrane electrolysis (PEMEL). Its benefits are a much smaller footprint, higher current densities and high-pressure capability. The anion exchange membrane

electrolysis (AEM) is the least mature of all water electrolysis concepts. It promises a highly disruptive cost advantage due to the very mild alkaline electrolyte and consequential use of less noble catalysts.

Due to operation at temperatures below 100 °C, the aforementioned technologies fall into the class of low temperature (LT) electrolysis. While LT electrolyzer systems display electrical efficiencies of 50 to 70% with respect to the lower heating value (LHV) of the produced hydrogen, high temperature (HT) electrolyzer systems with solid oxide electrolysis cells (SOEC) achieve electrical efficiencies of up to 84% (LHV). This is a consequence of faster kinetics of the thermally activated electrochemical processes and favorable thermodynamics at elevated temperatures [3]; molar Gibbs energy of reaction drops from ca. 1.23 V at room temperature to ca. 0.95 V at 900 °C while reaction enthalpy remains almost constant at 1.3 V [5]. As such, part of the energy required to split the water molecules (ΔH_f) is supplied in form of heat ($T\Delta S_f$), which in turn reduces the electrical energy demand (ΔG_f), see Fig. 1. Thus, SOECs have an edge

^{1,2}Marius Mueller (marius.mueller5@de.bosch.com), ¹Dr.-Ing. Markus Klinsmann  <https://orcid.org/0000-0001-8013-3599>,

¹Dr.-Ing. Ulrich Sauter, ¹PhD Jean-Claude Njodzefon, ²PD Dr.-Ing. André Weber  <https://orcid.org/0000-0003-1744-3732>

¹Robert Bosch GmbH, Corporate Research, Robert-Bosch-Campus 1, 71272 Renningen, Germany.

²Karlsruhe Institute of Technology (KIT), Institute for Applied Materials – Electrochemical Technologies (IAM-ET), Adenauer-ring 20b, 76131 Karlsruhe, Germany.

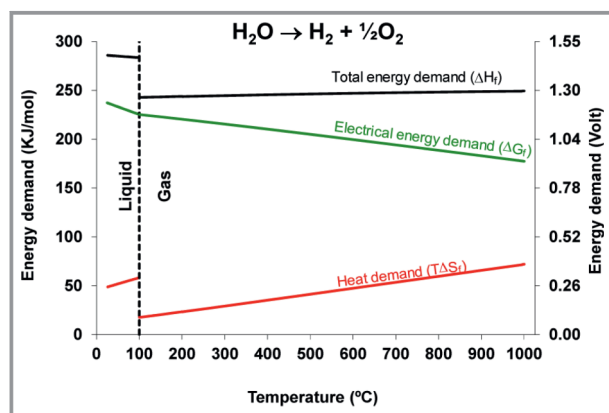


Figure 1. Thermodynamics of H_2O electrolysis at atmospheric pressure (calculated from data in [8]) [9].

over LT concepts in scenarios where the levelized cost of hydrogen is dominated by electricity costs. A further and important advantage of an SOEC is that it can be operated in reverse mode as solid oxide fuel cell (SOFC) to directly (re)convert stored hydrogen to electricity. As such, they are referred to as solid oxide cells (SOCs). Considering renewable chemicals and synthetic fuels, SOECs do not only split steam to produce hydrogen, but can also be operated with carbon dioxide/steam mixtures to produce a wide variety of syngas compositions as well as carbon monoxide [6, 7].

Development of SOEC technology, be it to improve performance or lifetime, requires an in-depth understanding of all relevant physical processes involved. Since some processes are hard to grasp by the sheer look on measured data and others are even impossible to resolve experimentally, adequate models for the different spatial and temporal scales of interest are vital to achieve the desired improvements. In this contribution, we will therefore first give a general overview on cell concepts and materials used in today's SOECs and then focus on the different types of models employed in literature and the distinct problems they address.

2 Solid Oxide Electrolysis

2.1 Operating Principle

The basic mechanism of an SOEC operated in steam/hydrogen mode is the splitting of steam to hydrogen and oxygen driven by an electrical current. The oxidation and reduction reactions are thereby spatially separated through an oxygen ion conducting, but electronically insulating, gas-tight electrolyte. At the fuel electrode steam is reduced to molecular hydrogen and oxygen ions. The latter are transported through the electrolyte to the oxygen electrode. Here, the oxygen ions react to form molecular oxygen. In the

reverse direction, i.e., in operation as a fuel cell, the reactions and transport directions switch, with reduction now taking place at the oxygen electrode, oxidation proceeding at the fuel electrode and oxygen ions moving from the former to the latter (Fig. 2).

As an endothermic reaction, steam electrolysis requires energy to split water into hydrogen and oxygen. The total energy demand per number of water molecules split thereby slightly increases with temperature (Fig. 1). Substantial part of the total energy demand can be provided by heat, including the unavoidable heat generated from internal losses. The state at which the heat from internal losses just balances the heat sink maintained by the endothermic reaction marks a special operating condition, the so called thermoneutral point. Operation of SOECs at the thermoneutral point or voltage (1.29 V) means no external heating or cooling is needed, which enables not only very high system efficiencies but also avoids balance of plant components for heating and cooling. When operated above the thermoneutral voltage, surplus heat is generated, which requires external cooling and thus lowers the efficiency. This is the case for all kinds of low temperature electrolyzers commonly operated at voltages between 1.5 and 2.5 V. On the opposite site, when operating below the thermoneutral voltage, the SOEC is cooling down and heat has to be supplied from external sources to maintain the operating temperature.

2.2 Designs

All SOCs consists of at least three functional layers—the fuel electrode, electrolyte and oxygen electrode (Fig. 3). They can be arranged in a tubular or planar cell design of which the latter is more common for SOECs. Depending on which layer provides mechanical stability, SOCs can be differentiated between oxygen electrode supported cell (OESC) or fuel electrode supported cell (FESC) [10, 11] (Fig. 4a), electrolyte supported cell (ESC) [12], metal supported cell (MSC) with a metal support on the fuel electrode side [13–16] (Fig. 4b) and inert substrate supported cell [17, 18]. The various cell designs come with characteristic advantages and disadvantages [19]. FESC enable low operating temperatures ($\leq 750\text{ }^\circ\text{C}$) due to thin electrolytes ($\leq 10\text{ }\mu\text{m}$)

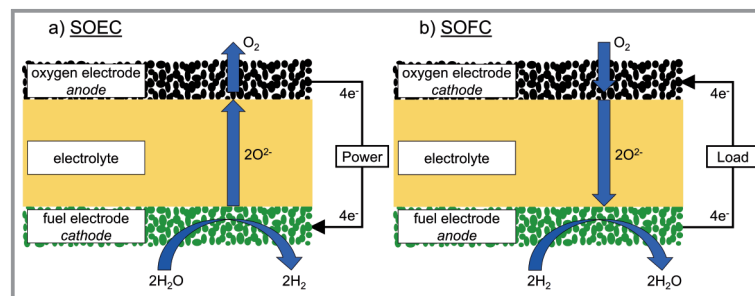


Figure 2. Operation principle for a) SOEC and b) SOFC mode.

and consequently small Ohmic losses in the electrolyte. However, a high gas transport resistance in the porous fuel electrode results from its comparatively large thickness (ca. 300 μm). For both FESC and MSC, reoxidation of nickel in the fuel electrode can pose a critical threat to lifetime, while ESCs are more redox-tolerant due to the thicker (ca. 150 μm) electrolytes and thinner electrodes [20]. On the other hand, ESCs require higher operation temperatures (750 to 900 $^{\circ}\text{C}$) to enhance the ionic conductivity of the thick electrolyte and keep the related Ohmic loss in a tolerable range. Such elevated temperatures impose challenging requirements in the choice of system components and compromise stack lifetime. MSC intrinsically need to be operated at lower temperatures ($\leq 650^{\circ}\text{C}$) [14–16] to avoid corrosion of the metal substrates. MSC substrates offer the best mechanical robustness among the different SOEC concepts but are of much lower maturity than FESCs and ESCs.

2.3 Materials

The characteristic property of an SOC electrolyte material is a highly ionic and ideally vanishing electronic conductivity. Mostly oxygen ion conductors are employed whereas proton conductors are still in development with no commercially available products yet. Furthermore, the electrolyte must be gas-tight to avoid leakages and should be chemically stable in both oxidizing and reducing atmosphere. State of the art materials fulfilling these requirements are of fluorite-type e.g., yttria or scandia stabilized zirconia (YSZ, ScSZ) today applied in most SOCs. Despite the better ionic conductivity of ScSZ, especially at operating temperatures below 700 $^{\circ}\text{C}$ [21], YSZ is more common due its lower price. Gadolinium or samarium doped ceria (GDC or SDC) are also potential electrolyte materials that show even higher ionic conductivities. However, as a result of the partial reduction of ceria in reducing atmosphere, the electronic conductivity of these materials becomes non-negligible and an additional electron blocking layer is necessary [22].

Furthermore, there are a number of compounds under investigation such as Er-stabilized Bi_2O_3 [21] or LaGaO_3 -based perovskite-type oxides [21, 23] that are still far from application into commercial products.

SOC fuel electrodes generally consist of a porous composite of a ceramic, ionic conducting phase and a metallic, electronic conducting phase in a so-called cermet. To enable electronic, ionic and gas transport the three phases have to be continuous. The most common cermet used for SOCs is a composite of nickel and YSZ. In these electrodes, the electrochemical reaction takes place at the

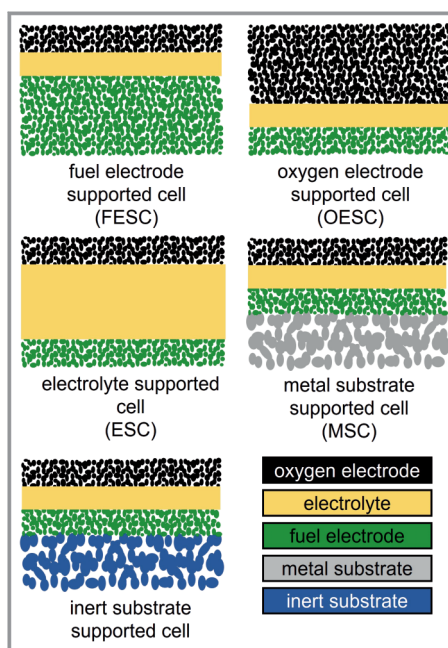


Figure 3. Schematic illustration of different solid oxide cell types.

three-phase-boundaries (TPB) between gas, electronic and ionic conducting phase. Besides conducting electrons nickel functions as an electrocatalyst for the electrochemical conversion of the fuel. Efforts to improve the electrode performance are leading to replacement of YSZ by GDC or SDC. These single-phase materials become mixed ionic electronic conductors (MIEC) in reducing atmosphere. Applying MIECs as fuel electrode material, available reaction sites are extended to the double-phase-boundaries (DPB) between gas phase and MIEC surface. This leads to higher tolerance with respect to carbon deposition [24] and sulfur poisoning [25] since these are catalyzed by nickel as well as the reac-

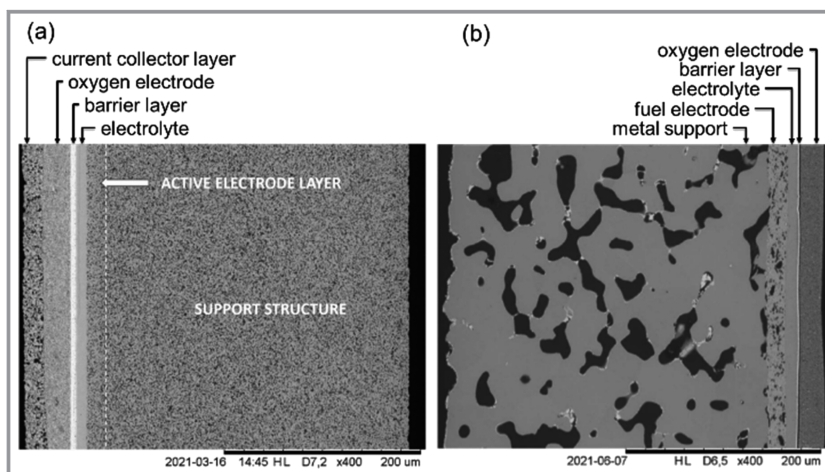


Figure 4. Scanning electron microscope image of the cross section of a) state of the art fuel electrode supported reference cell and b) metal supported cell [14].

tion continues to take place at the DPB despite deactivation of the TPB. Furthermore, an enhanced durability is achieved as Ni-agglomeration affecting the continuity of the Ni-matrix and thus the electronic conductivity can be compensated by the electronic conductivity of the ceria phase.

For oxygen electrodes composite materials consisting of LSM ($\text{La}_{1-x}\text{Sr}_x\text{MnO}$) as a catalyst for oxygen reduction or oxidation and an ionic conductor like YSZ or GDC were preferably used. In the last decade MIEC perovskites became the state-of-the-art oxygen electrode material. MIEC properties of these materials allow high performance single-phase electrodes. LSCF ($\text{La}_{1-x}\text{Sr}_x\text{Co}_{1-y}\text{Fe}_y\text{O}_{3-\delta}$) and LSC ($\text{La}_{1-x}\text{Sr}_x\text{CoO}_{3-\delta}$) are frequently used while other perovskite types like lanthanum nickelates are also investigated, as they show promising results in terms of degradation and material availability [26]. In order to avoid formation of low conducting mixed phases between those MIEC oxygen electrode materials and zirconia-based electrolytes, a doped ceria-based interlayer has to be integrated [27].

2.4 Stacks and Systems

The smallest functional SOE-unit is the single cell commonly operated at current densities of several 100 to 1000 mA cm^{-2} corresponding to hydrogen production rates of ca. 0.7–7 NmL min^{-1} at a cell voltage of 1.3 to 1.5 V. To produce technically and economically relevant amounts of hydrogen or its derivatives, hundreds of SOECs are connected in series into a stack. These stacks present the next higher functional unit, with power ranges between 1 and ca. 40 kW [11]. Multiple stacks can be combined into larger systems. Power inputs of such systems are currently between hundreds of kW to even the MW range with projects in different stages of realization.

In 2019 Salzgitter Flachstahl GmbH and Sunfire GmbH commissioned a 720 kW SOE system within the project GrInHy2.0, making it the world's largest SOEC installation at that time. The system achieved an efficiency of up to

84 % (LHV) and a hydrogen production capacity of up to 200 Nm^3 per hour. Integration into steelmaking operation was realized by using waste heat of the steel production to generate steam [28].

Within the MultiPLHY project, the world's first multi megawatt SOE system with 2.6 MW nominal power is built. The system by Sunfire GmbH is integrated in Neste's renewable products refinery in Rotterdam. It consists of twelve modules with commissioning starting in June 2023 [29].

A 1 MW SOE demonstrator is planned by Ceres Power Holdings, Robert Bosch GmbH and Linde AG to showcase the technology for green hydrogen production. The two-year operation starts in 2024 [30]. Topsoe A/S and First Ammonia LLC agreed on building the world's first commercial-scale green ammonia production. The two companies agreed on the installation of 5 GW SOE capacity with 500 MW already allocated to sites in Germany and the US with operation planned to start in 2025 [31].

Further, a commercially available application of SOEs for on-site production of CO via CO_2 electrolysis called eCOs[trade] is distributed by Topsoe A/S. Resulting from on-site production, transport and storage of carbon monoxide can be avoided. One stand-alone unit produces up to 100 Nm^3 of high purity CO gas per hour, with parallel operation of multiple units and thus an increase of capacity possible [6, 7].

The largest SOE system to date is installed by Bloom Energy at a NASA research facility in California. The 4 MW system is capable to produce more than 2.4 metric tons of hydrogen per day [32]. Bloom Energy reports to have an annual production capacity for SOEs of over 2 GW, with over 1 GW of SOE systems already deployed [33].

3 SOC Modeling

Understanding the complex, performance and lifetime limiting processes happening inside of a solid oxide cell (Fig. 5), and how they are affected by design parameters (materials,

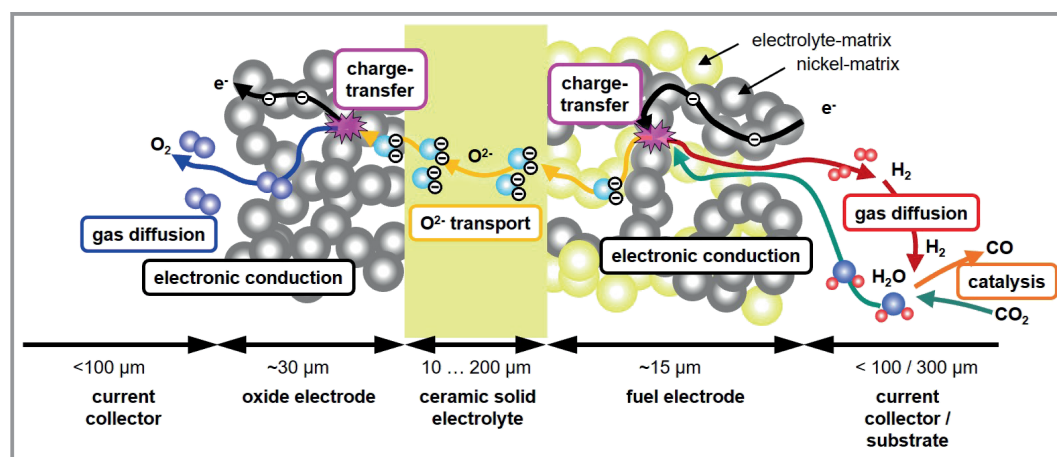


Figure 5. Processes in a SOEC.

microstructures, cell and stack layout) and operating conditions, is crucial for a systematic improvement of the overall performance and lifetime. On the technically meaningful stack scale, the distribution of the relevant internal fields, such as, temperature, current density, hydrogen flow, etc., and the related gradients have to be considered.

However, observation of most of these processes and fields by experimental means is often limited. For example, in-operando measurements of temperature distribution or local gas composition may be hampered due to spatial constraints or only possible on lab-scale cells. In other cases, e.g., for microscale processes like charge transfer reactions, direct measurements are even entirely infeasible with today's measurement equipment.

Thus, to fundamentally understand the causes and effects of the processes involved, as well as interaction between them, physical modeling is indispensable. Once such models are developed and validated, optimization of an SOC, e.g., via the design, material choice or operation strategy, becomes cheaper and faster compared to performing experimental variations. Yet, to accurately predict the behavior of a real system under changes of the operating conditions or for variations in the design or material properties, all relevant physical processes must be considered. In case of SOCs

and SOC stacks, this is a challenge as countless coupled processes (Fig. 6) take place over a wide range of time and length scales (Fig. 7).

Over the last years many studies with focus on different aspects of SOC modeling have been conducted. These models differ in the processes being considered, the implementation approach being used and their scope and application. A comprehensive overview over different processes and aspects of SOC modeling is given in the following.

3.1 Model Scopes

The scope of a model depends on the problem being addressed. On the highest level, this can be the question whether the immediate performance of a cell shall be studied or whether rather long-term behavior and degradation is in the focus. Further differences may lay in the spatial and temporal scales of interest (Fig. 7). For example, to which detail one wants to resolve the distributions of the various chemical species, temperature, voltage or current density. All these choices determine the number of the physical, chemical, mechanical, thermal, electrical, or electrochemical processes that the model needs to take into

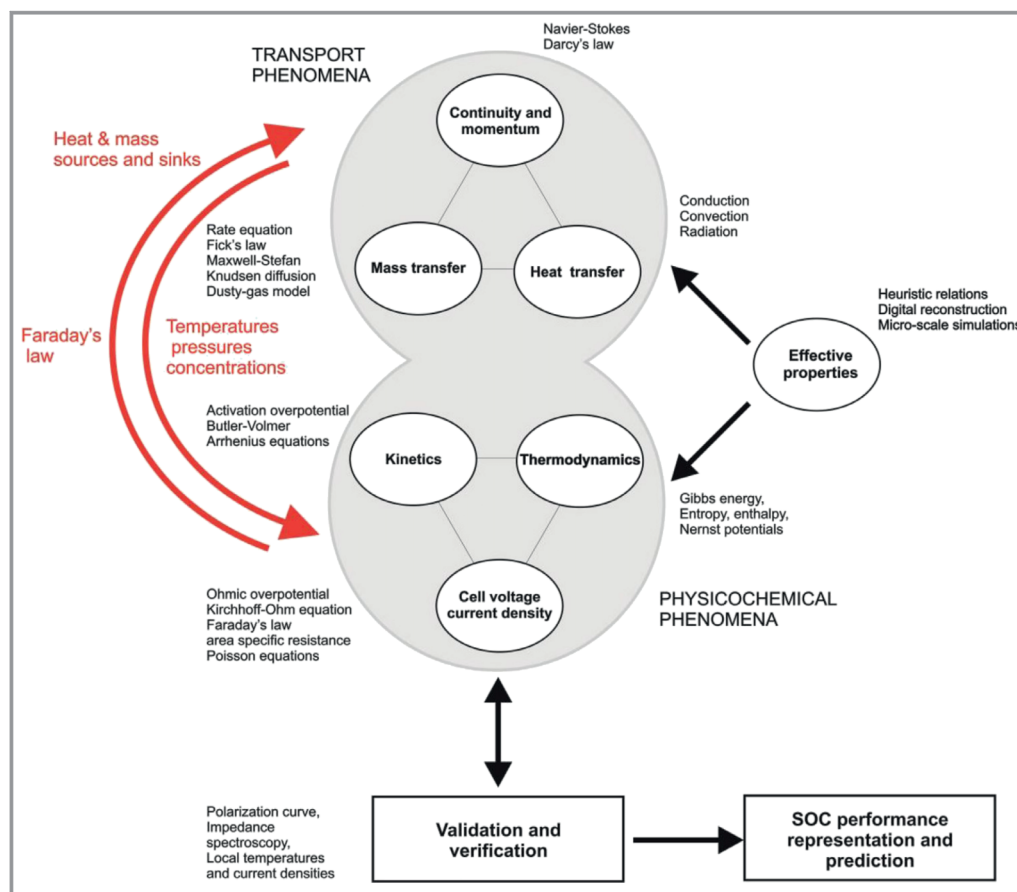


Figure 6. Modeling scenario for SOCs [34].

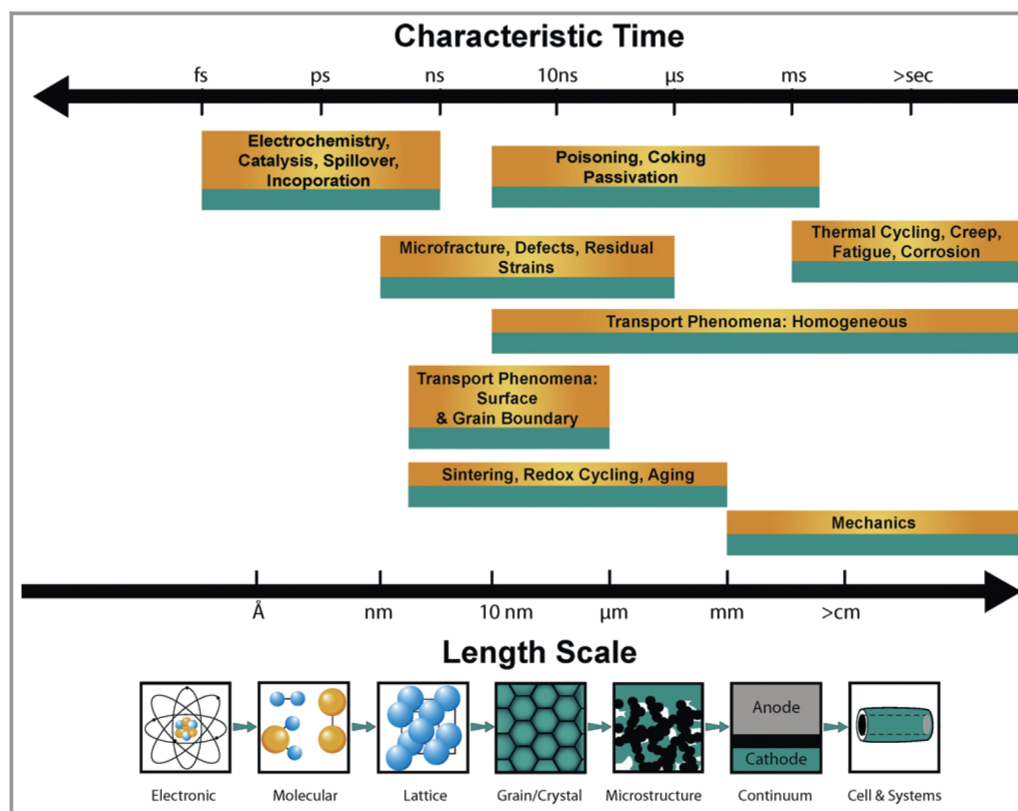


Figure 7. An overview of the time and length scales characteristic of functional and degradation processes in the heterogeneous SOFC electrode structures. The time and length scales provided are conceptual and are only intended to be characteristic of the scales at which these processes generally present themselves [35].

account as well as the spatial and/or temporal resolution that needs to be covered. In the following sections, various modeling scopes are discussed. Starting at the electrode level, the modeling scope expands by the number of processes included, going all the way up to fully coupled stack models and transient behavior.

3.1.1 Electrode Level

A detailed electrochemical model to determine cell voltage in dependence of operating conditions must depict the processes occurring at the electrodes (Fig. 5). These processes involve reactions, as well as the transport of species and charges, and typically induce overpotentials that lower the voltage of a cell to values below the open circuit voltage computed in thermodynamic equilibrium. To determine the respective overpotentials, different approaches are taken.

3.1.1.1 Kinetics

The electrochemical reactions at the electrodes are fundamental for the functionality of SOCs and must thus be described correctly in a model. Resolving the reaction mechanism down to the elementary reaction steps can support materials development and provide fundamental infor-

mation about microstructural designs of porous electrodes [36–38].

In most cases it is sufficient to consider the global electrode reaction by a single rate-limiting elementary reaction. An approach often used for modeling is applying a Butler-Volmer (BV)-type equation for each electrode [39]. It incorporates activation losses and is applicable over a wide range of operating conditions [40–42]. In contrast, the Tafel equation [43–45] or linear [43–45] approaches are less accurate at low and high current densities respectively.

Authors tend to simplify BV-type equations by setting the charge transfer coefficient to a fixed value of usually 0.5 [46–53] or using a hyperbolic sine function [54–57], often without deeper considerations on whether this is appropriate for the respective cell modeled. Another simplification sometimes found is neglecting the dependence of the exchange current density on the gas composition [46, 47, 49, 52, 58, 59]. These simplifications limit the applicability of model to scenarios, where gas compositions are similar to those of parametrization [60]. A demonstration how charge transfer coefficient and the dependence of the exchange current density on the gas composition can be determined is given in [40].

Utilization of the BV equation in models for SOCs is not undisputed, since it involves multiple assumptions that may

not be entirely fulfilled. The BV equation is defined for a single step single electron transfer reaction, while for SOC electrodes the reactions consist of multiple steps and multiple electrons are transferred. Often these individual reaction steps are combined in one BV-equation and described by effective parameters. The rate determining step is not always known and may also change with varying operating conditions [41, 42]. Further doubts on the applicability of the BV equation are formulated in [61].

Other approaches to couple reaction rate and activation overpotential are the Chang-Jaffé equation [62–64], assuming a linear dependency between activation overpotential and current [65, 66], or the approach presented in [67] and applied by [68, 69]. [70, 71] apply an elementary step description for the fuel electrode and BV equation for the oxygen electrode.

To account for the different catalytic reactions occurring when running the SOFC with reformat fuels, coupled elementary heterogeneous kinetics were studied in [39, 72, 73]. Internal reforming reactions were also investigated in [74]. As this review aims to elaborate on the production of hydrogen, an in depth look on the kinetics of reformat or CO/CO₂ operation is not carried out. The reader may instead refer to [75].

Another variation with respect to how the electrochemical reaction is implemented in the models, is the location assumed for the charge transfer to take place. In order to reduce implementation and computational effort, many models position the electrochemical charge transfer reaction at the interface between electrolyte and electrode and implement it as an interface condition [39, 50, 51, 55, 60, 76–86]. This simplified picture can be enhanced by assuming the charge transfer to be homogeneously distributed in the electrode in combination with a model to determine TPB density [58, 87–90], an approach that increases the complexity of the model and demands for a finer spatial resolution of the electrode. Detailed investigations on the distribution of the electrochemical active zones in the functional layers are presented, for example, by [91, 92] showing considerable change in the distribution of charge transfer current density respectively reaction rate in through-plane direction along the gas channel. In this context, also so-called transmission line models (TLM) [93, 94] can be employed for electrode materials, like for example Ni/YSZ [95–97]. In addition to the ionic and electronic pathways, in [97] also the gas diffusion resistance is incorporated in the model. Applicability of TLMs for a 2D model of gas channel and cell is presented in [98].

Oxygen electrodes are usually made of MIEC materials in which oxygen incorporation and removal occur over the entire surface of the porous microstructure. This raises the complexity of the interplay between oxygen exchange

kinetics, microstructure and diffusion. Therefore, kinetics and 3D microstructural models are directly coupled to enable distinction between microstructural and material influences on the electrode behavior [64, 76, 99–106]. An overview on oxygen electrode modeling is given in a recent review by [107].

3.1.1.2 Microstructure

Electrode microstructure has a strong influence on most of the relevant processes involved in an SOC, e.g., gas diffusion, electronic and ionic conduction, and conversion of species at reaction sites. Therefore, microstructural properties heavily impact performance and degradation of a SOC. The optimal electrode combines a high availability of active reaction sites with low resistance to gas transport, fast electron and ion conduction as well as low degradation in operation.

For the sake of simplicity, the complex three-dimensional microstructure of an electrode is often not directly accounted for. Instead, macro-homogeneous modeling approaches are being used, where the complex microstructure is described by volume-averaged structural parameters, such as porosity, tortuosity, specific surface area or volume specific length of the TPB. These values are then used to calculate effective macro-homogeneous transport properties. Examples are effective diffusion coefficients or effective conductivities [108–111].

Three different types of methods can be applied to determine characteristic structural parameters of a porous microstructure. An experimental method to determine all parameters of a real microstructure is the focused ion beam – scanning electron microscope (FIB-SEM) tomography [112] with which part of the electrode volume is reconstructed from sequentially recorded cross section images (Fig. 8).

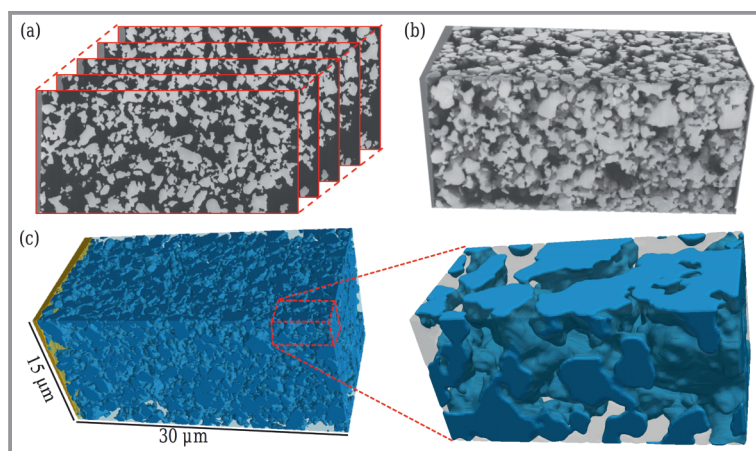


Figure 8. Different steps of 3D reconstruction: a) By stacking and aligning the 2D images in 3D space and b) expanding the pixels in the slicing direction, a 3D reconstruction consisting of voxels is derived. c) By assigning each voxel of the structure its corresponding phase, a 3D material distribution of the sample is obtained [113].

This destructive method requires time, experience, special equipment and well-prepared samples with the microstructure of interest. All these requirements are not often available to the model developer. Therefore, alternate ways to obtain microstructural parameters are applied.

A popular method to determine the microstructural properties of TPB length and effective conductivities for given volume fractions and particle size is the *percolation theory* [114]. Based on coordination number, percolation probabilities for the formation of connected conduction pathways consisting of particles are estimated. For this approach porosity is given by the respective volume fractions while tortuosity is either set to a certain value [47, 109, 115] or calculated with porosity-tortuosity-correlations such as the Bruggeman correlation [92, 109, 116–118].

One of the earliest studies to predict the microstructure for a cermet electrode was published by [119] investigating a mix of two particle species, either purely ionic or electronic conducting. [116] extended the approach to multi-component particle mixtures while also including the contact-number conservation requirement. A third phase to control the porosity and polydisperse powders were added by [120]. [118] extends existing models by considering surface area within a specific distance of the TPB as electrochemically active. Nano-particle infiltrated electrodes were characterized in [121]. A combination of percolation theory with a mesoscale microstructure model was presented in [92, 122].

Instead of using an analytical expression to derive microstructural parameters it is possible to computationally generate a microstructure for specified powder characteristics. Approaches with parameters derived from real microstructures are presented for a small section or real microstructure in [123] and for a stochastic geometry in [124]. To eliminate the need for empirical correlations and adjusted parameters, [87] generated a 3D microstructure with a drop-and-roll packing algorithm considering size distribution and composition of the powder. Effective transport properties were then determined with a Monte-Carlo random-walk method.

[55] presents a truncated pluri-Gaussian random field method [125] where the two solid phases are separately created as random fields and then joined. Further, a sphere-packing algorithm is presented with densification prescribed by continuously adding further overlapping particles and then modified to form a smooth surface [126]. For both approaches, comparison to a 3D reconstructed microstructure shows good agreement for relevant structural parameters like tortuosity and TPB length.

To derive average parameters from a microstructure a sufficiently large volume size, a so-called representative volume element, is necessary to limit the influence of the applied boundary conditions on the parameter values [127]. Also choosing periodic boundary conditions on the lateral boundaries was found to more closely approximate actual values [128].

The influence of microstructural parameters on cell performance and their optimal values were investigated in sev-

eral works. Varied quantities are, for example, particle size [47, 92, 118, 122, 129], porosity [47, 92, 129, 130], volume fraction [47, 92, 118, 122, 131] and functional and current collection layer thickness [109, 129]. Moreover, the concept of functionally graded materials, i.e., spatially varying microstructural properties of the electrodes, was investigated by [74, 88, 108, 130].

3.1.1.3 Mass Transport

For a continuous operation of an SOC the supply of reactant gas to the reaction sites must be ensured. Species are transported through gas channels and the porous structure of the electrodes. These domains have to be distinguished to adequately describe the gas phase transport in a model. Here conservation of mass is implied as well as incompressible ideal gas behavior.

In gas channels advective mass transport dominates as a result of relatively high flow velocities in the range of m s^{-1} [39]. Diffusion is therefore neglected most of the times with mass transport in the gas channels being described as a consequence of momentum conservation in form of Navier-Stokes equation (NSE) [60, 62, 65, 79, 88, 91, 132]. Further simplification is possible by describing gas flow in the channels with the assumption of negligible concentration gradients and velocities perpendicular to the gas flow direction. This can be motivated by the comparatively small height and width of the channels. Based on this assumption gas flow in the channels is reduced to a 1D problem [39, 85, 87, 89, 133–135].

As presented in [133], axial diffusion along the gas channel should not be neglected if convection and diffusion velocities are in the same order of magnitude due to low inlet flow rates. Since here, only molecular diffusion is present, either Fick's model for a single-component system or a Stefan-Maxwell model for a multi-component system is suitable [136]. The combination of NSE and Stefan-Maxwell model is suited [136] and adopted in [51, 58, 70, 71, 83] while others apply the Convection-Diffusion equation for the combined species transport by diffusion and convection [137–140].

Regarding the implementation of momentum conservation in porous electrodes, various approaches are presented. One possibility is to extend the NSE with a Darcy's law term [52, 53, 57, 62, 65, 86, 91, 137, 138, 140–143]. [58, 88, 90, 91, 122, 144, 145] apply forms of Brinkman equation, while [60, 71, 79, 146] replace NSE with Darcy's law and [83, 147] rely on the implementation in the dusty-gas model. The permeability needed for the Darcy's law term is determined via the Kozeny-Carman equation [51, 88, 141, 148, 149].

For cell types other than ESCs, mass transport resistance in the porous electrodes or substrate is significant, resulting in a concentration gradient between gas channel and reaction site which lowers the cell voltage. To consider this polarization contribution, the concentration of species at the reaction site must be determined. Simplified analytical expressions for the concentration profile in the electrode can be applied by

assuming a linear [40, 56, 150, 151] or exponential [54, 150] profile or using a limiting current expression [152, 153]. A more detailed insight into the species distribution at the reaction site is obtained using mass transport models that spatially resolve the species concentration.

An overview of common models for mass transport in porous electrodes, including their advantages and limitations, is given in the following.

Fick's model (FM) is the simplest approach to account for diffusion in porous electrodes. The model is limited to binary mixtures or diluted solutions without taking into account multi-component mixtures and Knudsen effects [154–158]. Knudsen diffusion accounts for interactions with pore walls and thus brings in a dependence on the actual microstructure of the porous materials. It should be considered, when the mean free path of typical gas components is in a similar range as the average pore radius of the structure, as is the case in the porous electrodes of an SOC [40, 41, 58]. Yet, incorporating Knudsen diffusion by using the Bosanquet formula [159] is not recommended by [158], as the assumptions for the Bosanquet equation are not met in an SOC. This may lead to serious inconsistencies in the determination of the diffusive fluxes.

The Stefan-Maxwell model (SMM) extends the FM towards multi-component mixtures. Interactions between all species, as well as thermal and pressure diffusion is taken into account [160, 161]. However, it does not consider Knudsen diffusion, pressure gradients and momentum balance [158]. Implementing Knudsen diffusion through the Bosanquet approach in the SMM model should be avoided for the same reasons as for the FM.

The dusty-gas model (DGM) was proposed by [162] as a model to describe gas transport in porous media. In addition to interactions between multiple species like the SMM, it includes interactions of gas molecules with pore walls, i.e., Knudsen diffusion as well as Darcy's viscous flux.

As shown by [158] it is important not to set a uniform pressure condition or apply Graham's law when implementing the DGM since it is incompatible with systems in which reactions occur. [163] generalizes the DGM by inclusion of a pore size distribution and thus eliminates the assumption of a single pore-size. A simplified application by reformulating DGM in form of FM is presented in [164], showing very good agreement to the original DGM.

Criticism about inconsistencies in the derivation of the DGM has been expressed in [165–167]. However, comparisons of the DGM to more complex models like Binary Friction model (BFM) [165] and cylindrical pore interpolation model (CPIM) [166] show only small differences and thus confirm the practical applicability of the DGM [157, 168].

Multiple publications compared the different diffusion models concerning their capability to predict gas phase mass transport in porous electrodes [136, 157, 169–171].

In terms of the computational effort associated to the models SMM ranks best, followed by the DGM and the even more costly BFM [157].

In [136] it is found that the DGM provides a more accurate prediction of the concentration overpotential than the SMM, particularly for high current densities. [170] derives analytical formulae for the diffusion resistance obtained from employing FM, SMM and DGM and compares them with experimental impedance data, treating tortuosity as the only fitting parameter. In this comparison, only using the DGM results in a constant tortuosity for various operating conditions which demonstrates the superior suitability of this method to correctly predict the gas diffusion resistance of porous electrodes.

The good balance between computational complexity and accurate predictions is also reflected in the high number of recent publications applying the DGM to describe mass transport in porous electrodes [76, 79, 83, 91, 115, 122, 172].

The studies of [136, 157] show that a 1D approach to mass transport in porous electrodes is not able to represent measurement data with satisfying precision, regardless of the model used. They show that a 2D approach, combining SMM in the gas channel and DGM in the porous fuel electrode, is a more suitable approach to describe mass transport in an isothermal SOFC. The coupling between species concentration in the fuel channel and at the electrode surface is established by prescribing equally large fluxes at the respective interface [136].

In their 2D isothermal model, [172] also apply the DGM and additionally consider a simplified competitive adsorption and surface diffusion. This is done in a cell model with uniformly distributed active reaction sites in the electrode. Further investigation on surface diffusion is conducted by [117] elaborating its influence on the limiting current and [70].

Mass transport models require correctly determined diffusion coefficients to factor in the diffusive properties of gaseous species and their mixtures. For binary gas diffusion, the diffusion coefficient can either be determined through correlations like Fuller's method [173, 174] or by application of the kinetic-gas-theory with the Chapman-Enskog approach [174, 175]. In case of diffusion in a porous structure, the coefficients are corrected by the microstructural parameters porosity and tortuosity [176]. To include Knudsen diffusion, a pore radius dependent diffusion coefficient needs to be determined [176]. If diffusion coefficients are not determined via the above-mentioned methods, they can also be treated as free parameters and fitted to measurement data.

The presented mass transport models are applied in different forms to determine species concentrations at the reaction sites. Mainly DGM [42, 51, 54, 55, 60, 77, 83, 85, 86, 92, 132, 147] or SMM, either neglecting Knudsen diffusion [143, 146] or considering it with a Bosanquet formulation [58, 62, 88, 148, 177, 178], is implemented. FM is applied without Knudsen diffusion [142] or with Bosanquet formulation [145, 179] while the Convection-Diffusion equation is used either with [137, 138] or without [139]

Bosanquet formulation to describe species transport. For all models the coupling between mass flow rate through the electrodes, electronic and ionic current densities is described with Faraday's law assuming ideal Faradaic efficiency, side reactions do not have to be considered in SOCs. It should be noted that the gas–solid transfer might cause problems in some CFD-applications as the electrode acts as a mass source/sink where mass conservation is not fulfilled.

3.1.1.4 Charge Transport

For charge transport, charge conservation is considered. Resistance due to charge transport in the cell, referred to as the Ohmic overpotential, lowers the measured cell voltage. The Ohmic overpotential caused by charge transport in the electrolyte, which is assumed to be purely ionic, but also in the electrodes, is computed by applying Ohm's law [54, 56, 78, 90, 146, 147]. When considering non-ideal contact of the cell by an IC, an additional Ohmic contact resistance is introduced in some cases [54, 56, 83, 135, 146, 147, 152, 178, 180, 181].

3.1.2 Cell Level

Models on cell level describe the basic unit of any SOC system, either spatially resolving the relevant fields in through-direction of the different layers or along them (1D), or without any spatial resolution at all (0D). Essential target of these models is the prediction of the current-voltage (CV) characteristic of a cell. This is often done by subtracting analytically or empirically determined overpotentials from the theoretical, loss free cell voltage determined by the Nernst equation in an "OCV-losses model".

Other approaches on cell level include the derivation of an area specific resistance (ASR) from measured data [139, 182, 183] or replacement of overpotentials by physically meaningful electric potentials, which allow to consider multi-step reaction mechanisms as well as double layer capacitances [177].

3.1.2.1 0D Cell Models

If only the overall performance of the SOC is of interest, comparatively simple 0D models can be applied. A central assumption of these models are negligible gradients of the operating and boundary conditions, as well as of any other parameters, over the whole area of the cell. This is usually valid for small active areas of up to a few cm^2 and if negligible fuel and oxidant conversions can be assumed. Models in literature differ in the assumptions taken to describe loss processes and the specific parameter values used as summarized by [40].

With an increasing number of assumptions and simplifications, a model becomes progressively limited in its range of applicability. To predict cell performance in a wide operating range in hydrogen fueled SOFC mode, [40] adopts an approach with only few assumptions and determines all

necessary electrochemical parameters through electrochemical impedance spectroscopy (EIS) and subsequent equivalent circuit model (ECM)-fits. This approach was further developed by [184] and [41] to model CO/CO₂ and SOEC mode respectively. Other models predicting cell performance without spatial extension are presented in [43, 45, 155].

3.1.2.2 1D Cell Models

For technical application, cells with larger active area of several cm^2 and non-negligible gas conversion rates are more relevant. Consequently, the various gradients evolving under such conditions must be considered when modeling the cells. In a cell operated at a finite current, both gas composition and cell temperature change along the gas channel due to the electrochemical reactions taking place. As a result, Nernst potential, overpotentials, current density, and thus also ageing drivers vary as a function of the spatial position. Different approaches exist to take these variations into account.

In [185] data of a cell with small active area is collected in a map of experiments and scaled up to an active area of 16 cm^2 by calculating spatially distributed operating conditions. This procedure is again employed in [186] now using simulated data taken from the model of [40] instead of experimental data. Although in both cases an isothermal cell is assumed, the match of the predictions with experimental data from a larger cell is reported to be good. Stationary [46] and dynamic [187] SOEC operation are modeled with spatially resolved temperature distribution along the gas channel but using simplified expressions for the activation overpotential. Other studies also resolve spatial variations of the relevant variables and components along the gas channel for isothermal CO₂ electrolysis [188], non-isothermal SOEC operation [49] and reformat operation [39].

A combination of two 1D approaches to numerically model an isothermal SOC is presented by [39, 50, 177]. The gas composition along the channels is described by a set of 1D model equations, while a second 1D model is applied in direction of the cell thickness, yielding a quasi 2D model of the cell.

Further models examining the gradients in gas composition and potential through electrodes and cell are applied in the studies of [47, 129, 133, 189]. Special emphasis on the rate limiting reaction step was placed by [42], including detailed heterogeneous elementary reaction kinetics and electrode kinetics.

3.1.2.3 2D Cell Models

To resolve 2D distributions over the cell area, rotational symmetry is applied to model circular (button) cells both for the isothermal [55, 117, 141, 148, 172] and non-isothermal [68, 70, 71, 152] case. Performance is analyzed in isothermal models by implementation of detailed mass trans-

port models using DGM [55,141,172], incorporating surface diffusion [117,172] or adopting a modified SMM [148].

The gas composition in a button cell under direct internal reforming operation is studied in isothermal [141] and non-isothermal [152] operation. [68] focuses on temperature and concentration fields while [70,71] consider species distribution in the electrode resolving adsorbed species.

3.1.2.4 Thermal Modeling

Temperature impacts almost all processes going on in a cell. Hence, taking into account its spatial distribution increases the accuracy of the model's prediction but also raises its complexity significantly. The inhomogeneous temperature distribution prevailing in any SOC is a result of boundary effects, such as, heating and cooling at the outer surfaces, but also due to the uneven distribution of heat sources and sinks, such as electrochemical reactions or Joule heating from internal losses. Between spots of different temperatures, transport of heat occurs in form of conduction, convection and radiation.

Non-isothermal models generally include heat convection in the gas channel and heat conduction in the solid phase of the porous electrodes, as well as in electrolyte and interconnector (IC). In some studies, convective heat transport is also implemented in the porous electrode regions [57,58,60,137]. In other studies, it is argued that due to a Peclet number below unity, this process is negligible [54,152].

In [60,137,138,190–193] heat conduction is considered for all domains, including the gas phase. For porous electrodes heat conduction is included through volume averaged effective heat conductivities [54,57–59,70,92,142].

Convective heat transfer depends on the temperature difference between surface temperature and temperature of the gas and is applied to couple fluid and solid temperature in porous electrode. As a common assumption, it is often employed that the heat transfer between gas and porous structure takes place on a comparatively short time scale, so that solid and gas temperature equalize rather quickly and a local thermal equilibrium (LTE) is maintained [57–59,74,88,91,138]. The validity of the LTE assumption is shown in [194].

The available literature does not present a consistent picture with respect to the treatment of heat transport through radiation. Multiple publications neglect the influence of radiation, with some arguing that its contribution is small compared to other heat transfer mechanisms [74,83,195]. Discarding radiative heat transport significantly reduces computational effort as the complete description of radiation in a 3D setup requires seven nonlinearly coupled independent variables [196].

In an IC-contacted SOC, radiative heat transport occurs between various surfaces. Heat exchange by radiation between layers of the cell and gases or walls can be neglected

according to [197,198]. In contrast heat transport from surface-to-surface radiation between the electrodes and IC [46,54,80,85,142,152,199] and to the surrounding, as often implemented in form of boundary conditions [54,76,135,152,190,199], can be significant.

Radiation is typically modeled by the Stefan-Boltzmann-equation, assuming either a gray [46,54,60,80,85,135,142,152,196] or black [190,199] body behavior of the surfaces. Models that include heat radiation via analytical terms [200], using the radiosity method [196], or applying the Stefan-Boltzmann equation [142] find lower temperatures and temperature gradients compared to the case when radiative heat transport is neglected. Summaries of the literature concerning the modeling of heat radiation in SOCs can be found in [196,201].

Thermal models also differ by the choice of heat sources and sinks considered. The main heat source (SOFC) or heat sink (SOEC) is the reversible heat caused by the cell reaction. It is implemented in about every model. Depending on the resolution and homogenization level of a model, reaction heat is either attributed to the interface between electrode and electrolyte [51,60], the entire electrode volume [58,62,76,83,85,91,92,142,143,193,199,202] or to the whole cell domain [46,52,68,80,81,89,137,139,203].

Joule heating through Ohmic resistance is ascribed to the electrolyte and electrodes [80,137,193], where also heat from the activation potential is generated and considered in [51,52,58,68,74,85]. In [62,83,91,142,195,199] these heat sources are located in the respective layer in which they occur. The stack models of [191,192,204,205] combine all source terms into a fixed predetermined heat generation rate.

After correct implementation of the respective mechanisms for heat generation, consumption and transfer, appropriate boundary conditions have to be defined. For the description of the different boundaries, we refer to the orientation of the geometries in (Fig. 9). The stack layer consists of a periodic array of gas channel and rib perpendicular to the gas flow direction. To decrease calculation cost for the 3D case, the geometry is reduced to the cell domains plus either a single gas channel and rib section or half of it, the so-called repeating unit (RPU) (Fig. 9). In the 2D case, the RPU contains gas channels on either side of the cell cross section. The thermal boundary condition at the gas inlet is usually of Dirichlet-type, i.e., by prescribing the temperature. At the gas outlet, often a Neumann-type boundary condition is defined, with a temperature gradient of zero. An adiabatic boundary condition is applied for the cell and IC domains at the front and back faces [80,83,91,195,207]. To resemble the conditions in the middle of the stack, periodic, symmetric or adiabatic boundary conditions are used at the top and bottom boundaries of the modeled geometry. At faces on the left and right of a 3D geometry, either adiabatic [80,92], periodic [57] or symmetry [111,142] conditions are set. For 2D models along the gas channel [51,58,83,85,139,199] gradients perpendicular to

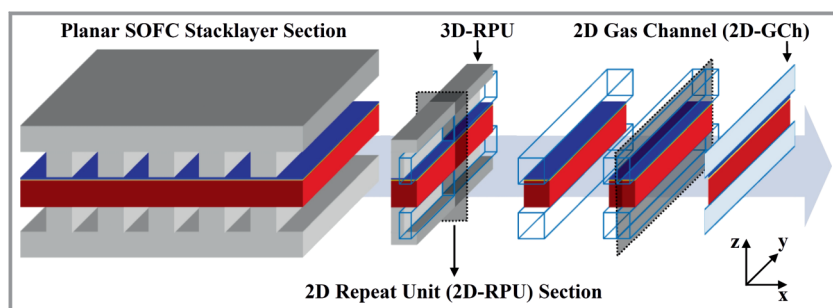


Figure 9. Breakdown of FEM model geometry development [206].

the modeled plane are neglected. As boundary conditions for the outer perimeter of stacks convection and radiation [85, 135], only convection [178], adiabatic walls [153, 191, 192, 208, 209] or isothermal walls [153] are set.

Detailed thermal studies for a RPU, including also the IC as a geometric feature of the model, are presented in 2D [83, 199] and 3D [80, 91, 195]. [91, 195] find significant influence of the thermal conductivity and thickness of the IC on temperature profiles in the cell. [83, 199] apply homogenization to include both rib and gas channel in their 2D geometry and carry out an extensive validation.

In contrast to modeling, approaches determining temperature distributions by measurements demand a high experimental and constructive effort and are thus only scarcely demonstrated in literature. Works that go through the endeavor mostly employ thermocouples [199, 210], while integrated thermocouple arrays [211] and fiber optical sensors [212] are also proposed.

3.1.3 Stack Layer

3.1.3.1 Mechanical Stress

An SOC stack is assembled by several components. In order to fulfill their respective function, different materials with the appropriate properties are chosen in their fabrication. Inherent to each material is a thermal expansion coefficient (TEC) that describes the materials dimensional change due to temperature variation.

In such a multilayer structure, thermally induced mechanical stress arises either due to an inhomogeneous temperature

distribution or due to a mismatch in the TEC of adjacent components, since in both cases an inhomogeneous volume change occurs. Hence, to properly investigate such stress, knowledge of the prevailing temperature distribution is required. This can be obtained by a separate multi-physics model [69, 144, 193], derived from measurements [210] or calculated for purely conductive or purely convective heat transfer [213].

In modeling of mechanical stress in SOCs, common and most simple assumption is an isotropic [52, 144, 179, 191, 193, 214, 215] and linear elastic [52, 144, 145, 178, 179, 191, 193, 210, 213] material behavior, as well as a linear and isotropic thermal strain [144, 145, 191, 193]. In the case of homogenization approaches as in [178, 213], the effective mechanical parameters for the homogenized materials become anisotropic.

Typical characteristic stress parameters related to material failure and fatigue considered in most studies are principal stress and von Mises stresses (Fig. 10). In models investigating the transient evolution of stress, also creep is considered [204, 213, 216, 217] except for [205].

Mechanical stress induced by TEC mismatch was studied for all stack components in [191, 204, 205, 210]. In these investigations sealant, frame and cell were considered as one domain. [52, 69, 179, 193, 216] resolve the stress distribution in cell layers with [145] additionally including the IC and [144] the sealings. The impact of residual stresses in the different layers of a cell [216] or stack [213] was studied using Bernoulli-Euler beam theory. Stresses inside Ni/YSZ fuel electrodes are studied in [218], considering sulfur poisoning [52] and regarding the redox process [123]. Occurring mechanical stress in the interface between glass sealing and Crofer 22APU was investigated in [215], [69] identified the electrolyte as weakest component due to its small extent and highest Young's modulus.

Assessing the risk of stress induced cracks in SOCs is crucial since they impair the performance of a stack and may finally lead to its complete failure. At stack layer level, a common way to determine failure probabilities is provided by the Weibull theory [216, 219–224], which applies to brittle materials like ceramics and takes into account the

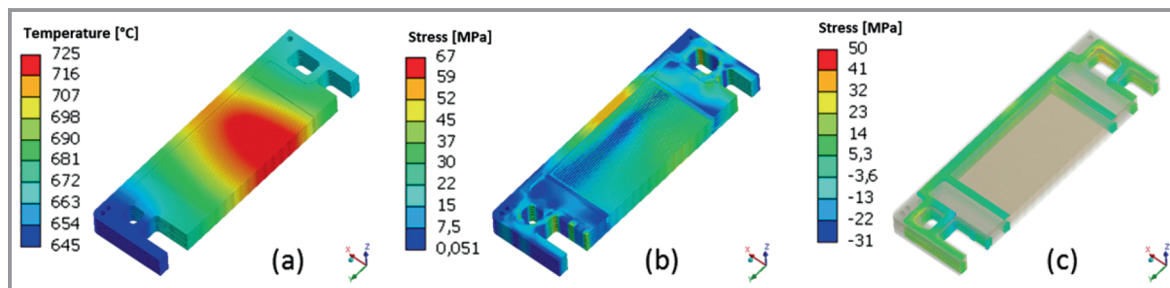


Figure 10. a) Temperature distribution of the stack; b) von Mises stress distribution of the steel components; c) maximum principal stress distribution of the sealants [205].

history of the mechanical load on the structure. These probabilities are computed for single cell layers either as an integral value [216, 220–223] or distributed over the area of a layer [224]. Impact of operating time [221–223], temperature or temperature gradients [216, 220], current density or power density [221–223] and layer thickness [216] on failure probability are evaluated.

Failure on stack level induced by redox cycles was investigated by [225] by applying a damage evolution law that accounts for changes in material properties due to microcracks and isotropic swelling. [226] uses a special localization approach in a multi-scale model including methods from classical fracture mechanics to identify the most critical spots for mechanical failure. Loss of gas-tightness, electrical contact and thermal buckling were investigated in [227].

The impact of delamination in on performance in SOEC mode was studied by [90, 228, 229]. Here, delaminated areas between electrolyte and oxygen electrode were treated as insulating layers for electronic and ionic currents.

3.1.3.2 Flow Field

In an SOC stack, cells and ICs are piled up alternately on top of each other. In this arrangement, ICs provide electrical contact between the cells and incorporate some kind of flow field that supplies the cells with the required gases. As these two functions pose different requirements to the geometry, optimization is needed to achieve best performance. Experimentally varying geometrical parameters is time and cost intensive. Hence, numerous modeling studies are conducted investigating and optimizing geometrical features.

To explore the impact of the IC design on cell performance, most often a rectangular, parallel channel design is considered. Therefore, in 2D studies a RPU perpendicular to the gas flow direction is sufficient, implicating that gradients along the gas channel are negligible [77, 78, 146, 180, 228, 230–232].

The resistance of the IC is hereby often neglected due to the comparatively high electrical conductivity of the material [146, 230–232]. In other works, it is explicitly taking into account using Ohm's law [77, 78]. The contact resistance at the interface between electrode and IC can be treated in a lumped expression [233], incorporated as an additional contribution to the ASR of the cell [146, 180, 228], set to an experimentally approximated value [230–232] or completely neglected [77, 78].

IC design not only affects the electrical contacting and resistance, but also the distribution of the relevant gases in the electrodes. Particularly in the porous electrode below the ribs, gas depletion is a known issue. For species transport in the porous electrode, FM [228], SMM [146] and [77, 78, 180, 232] DGM are applied. [230, 231] do not resolve gas depletion under the ribs and [233] neglects concentration polarization altogether. In contrast [77, 78, 180, 232, 234] fully resolve species distribution in the whole elec-

trode. To avoid numerical instabilities [146], and [132] for the 3D case, introduce an oxygen concentration threshold such that regions with low oxygen concentration are treated as purely electronic conducting.

An analytical expression for the effective ASR, both for a concept with channel and dimple structure, was derived by [233]. Optimal rib [146, 232] and gas channel width [230, 231], as well as current conduction and gas species transport [77, 78, 180], were examined in 2D for parallel gas channels.

To cover both the impact of the alternating ribs and gas channels and the varying conditions along the gas channel, the modeled geometry needs to be extended to a 3D channel RPU [53, 57, 59, 84, 91, 92, 122, 140, 142, 147, 195]. The species distribution in the electrodes in contacted areas along the gas channel is investigated for isothermal [53, 122, 147] and non-isothermal conditions [57, 143]. Additionally, in non-isothermal models, current density [57, 143], overpotentials [57] and temperature distributions [57, 84, 142, 143, 195] are resolved for the entire electrodes, including the areas under ribs. Further, modeling the channel in 3D allows for the examination of crossflow configuration for single channels [122, 143, 147].

Expanding the geometry to cover the whole cell area enables to investigate more complex serpentine [235] and alternative [132] flow field designs. In these full cell models, both co-flow [86, 137] and crossflow [62, 69, 137, 145, 182, 193] configuration can be studied.

3D modeling of large active area cells ($> 16 \text{ cm}^2$) with parallel gas channels is presented in [62, 69, 86, 137, 145, 182, 193, 235]. In these works, distributions of different fields of interest, including temperature [69, 137, 145, 182, 193, 235], species [69, 137, 145], current density [62, 69, 137, 182] and mechanical stress [69, 145, 193] are computed along the cell area.

Instead of explicitly resolving the flow field in the channel, [182] models the domain as an anisotropic porous material while [62] adopts a porous medium to model the contacting via Ni and Au meshes in a lab-scale cell. These two approaches therefore not provide information about local effects caused by the flow field. It is worth noting that of these 3D models, only [86] in their study of overpotentials use DGM to describe mass transport in the porous electrodes in detail.

When designing a stack, inhomogeneous distribution of gases should be avoided as it leads to non-uniform performance and degradation in and between different stack layers. Studies on the gas distribution and flow fields often solely implement mass and momentum conservation as governing equations [236–239], leaving away other multi-physical effects. This is justified by the work of [236] which finds only a minor difference for the gas distribution in the channels of a stack layer, when employing either a reacting non-isothermal or a non-reacting isothermal model.

Gas flow in the channels is considered to be laminar for fuel flow [214, 236, 239] and turbulent for air flow [236] as

suggested by the respective Reynolds numbers. Viscosity of the gas mixture is determined by Sutherland's law [236–238]. Wall boundaries are set as adiabatic [236, 238], no-slip [236–239] or via wall functions [236, 237].

Mass flow uniformity between channels of a cell layer and geometrical influences thereon are examined by [202, 214, 236]. Mass flow distribution depending on the manifold design is investigated for planar cell stacks [237, 239] and tubular stacks [238]. Using 3D stack models, a reasonable uniform mass flow rate is confirmed in [191], while [139, 202] find a maldistribution over the height of the stack.

3.1.4 Stack

A common simplification used to approximate the performance of a full SOC stack is the modeling of a single RPU located in the middle of the stack. When equipped with suitable thermal boundary conditions, e.g., of adiabatic or periodic type [83, 85, 92, 149], reasonably accurate predictions of the performance of a stack are demonstrated with this approach [83, 85]. However, the actual conditions at the boundaries of a full stack may have a noticeable influence on the distribution of the relevant fields within the stack [82]. Within a single RPU, such geometric effects can only be considered to a limited extent. The most critical manifestations of so induced inhomogeneities are, for example, hot spots and locations of fuel starvation. Conditions of this type provoke faster degradation and a decrease in performance and may be also act in a self-enforcing manner with respect to the uneven distribution of the physical fields in a stack. Spatially resolving local conditions with full stack models can thus help to detect optimized operating strategies, that avoid such repercussions.

Due to the various scales of the many processes taking place in an SOC, as well as the interactions between them, the computational requirements to compute a full stack in all detail is enormous. To realize the simulation of a full stack including its geometrical intricacies and the relevant boundary conditions, special approaches thus need to be taken. This can involve simplifications, such as, for example, neglecting or reducing certain effects or features, averaging over parts of the stack via homogenization techniques, or also hierarchical multi-scale methods.

3.1.4.1 Reduced Physics Models

Reduction of the computational demand and achieve sufficient numerical stability via less complex physical models can be accomplished in various ways. In [153, 240] the cell is reduced to a single layer, neglecting the porosity of the electrodes overall. [202] sets a uniform current density over the cell area and thus describes the electrochemistry only via source terms for the different species. Modeling the cell as one domain and considering the electrochemistry only via predetermined heat sources is presented in

[191, 192, 204, 205]. In these models the distribution of the different species is also not resolved. A different approach is presented in [81, 82], which combines electrolyte and oxygen electrode into one phase with appropriately adjusted parameters. Instead of resolving oxygen transport and current density distribution under the ribs by numerical means, analytical expressions are applied thus reducing the required number of mesh elements. Further reduction is achieved by relating the set operating current to the cell voltage for every cell thus avoiding to resolve charge transport in the interconnectors.

3.1.4.2 Homogenized Models

Volume-averaging is not only performed on a sub-electrode level to obtain microstructural parameters but is also applied to RPUs and large 3D geometries to reduce computational cost. In this approach, repeating geometries are substituted by homogeneous domains with equivalent transport properties [241, 242]. Comparisons of spatially resolved and homogenized models show similar results and thus validate the modeling approach [139, 242].

Instead of resolving the single ribs and channels of the IC, they are often substituted by an anisotropic medium with equivalent properties e.g., porosity and pressure drop. It is considered as porous medium, if species transport is included [209, 243] or as a bulk material, as, for example, in the thermomechanical study of [244].

To account for the difference in the transport pathways between the homogenized porous media and the real geometry, a correction factor for the geometry of the flow field is implemented in [243] and further investigated in [245]. A similar approach with a correlation factor is applied to heat transfer in a homogenized porous media in [246].

[199] applies homogenization to a 2D RPU along the gas flow direction to describe thermal behavior of both gas channel and rib in the same domain. This is done by adjusting the heat conductivity perpendicular to the gas flow direction to keep heat flux and temperature difference constant.

All individual RPU domains are homogenized by volume averaging in [139]. Combined with heat and mass transfer correlations the local effects near walls are represented without the need of a finely resolved mesh. Further, the entire electrochemistry of an SOC is implemented as an experimentally determined ASR. Comparison with a detailed numerical model demonstrates a good agreement, while calculation times are being cut down by almost two orders of magnitude. The model is further compared to experimental data in [201], displaying well-matching results with respect to temperature distribution and cell voltage.

[178] employs the volume averaging homogenization approach to all phases of a fully coupled stack (Fig. 11). A single homogeneous medium with anisotropic properties is obtained which represents the cumulative behavior of the individual RPUs at a macroscale. As one mesh element can

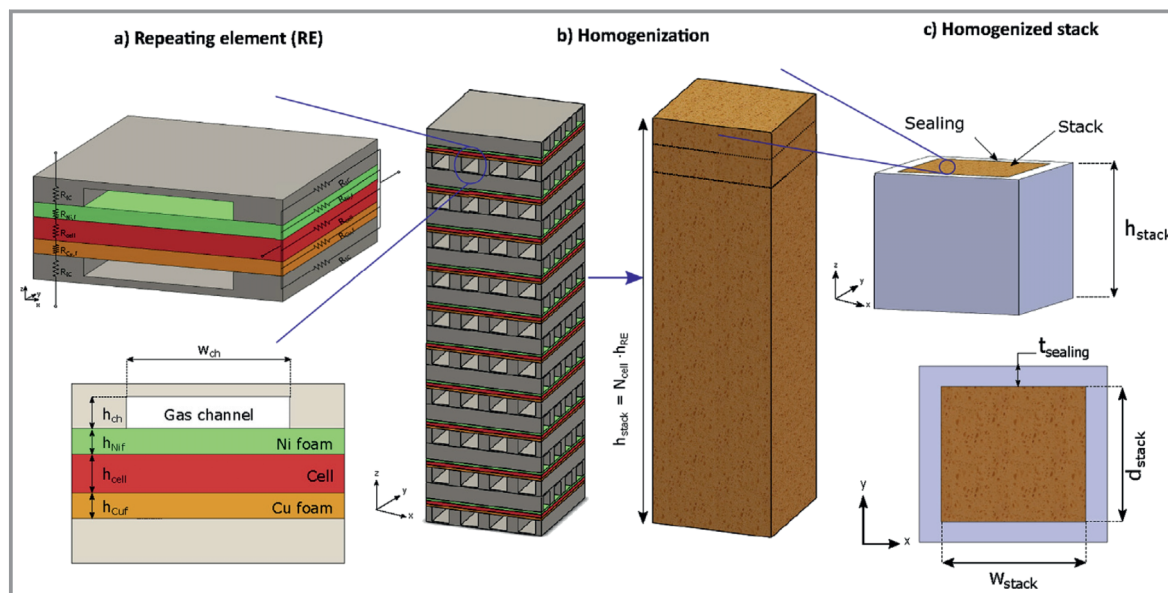


Figure 11. The stack geometry and homogenization: a) Repeating element of active part of the SOC stack in 3D and cross-section, b) 10 repeating elements stacked and the equivalent homogenous media and c) homogenized stack with two domains; active domain and manifold domain in 3D and a top view [178].

include multiple repeating units, less elements than cells are needed, leading to a significant reduction in computational time. This allows to model long-term degradation via inclusion of the governing equations in a transient form and addition of time-dependent evolution equations for the degradation phenomena [151].

3.1.4.3 Hierarchical Models

To compute the overall response of a full stack, while still maintaining insight into localized effects, models coupled on with different spatial scales can be employed. [226] follows this approach and uses sub-models with boundary conditions derived from a higher-level homogenized model to study and include fracture mechanics on a lower scale.

A different approach to limit computational effort needed for stack computation is applied by [135]. An agglomeration algorithm is used, which groups several RPUs into clusters according to the local stack temperature field. All RPUs belonging to a cluster are assumed to behave equivalently. After several agglomeration steps, multiple clusters are formed with a representative RPU for each cluster then being solved in detail.

3.1.4.4 Numerical Solution Strategies

Another important handle to reduce computation time and achieve stable numerical solutions, it the optimization of the numerical solution strategy. Solving for coupled fields is mostly done by iterative procedures. Step-by-step segregated solver approaches are presented in detail in [58, 82, 151]. First the fluid flow field is solved and then temperature field is solved second [58] or last [82, 151].

Modules solved in the middle are species transport and after that current distribution [58, 151] or vice versa [82]. In other models the thermal field is separated from the other fields and treated as an outer iteration loop to achieve convergence [54, 85, 135, 153].

3.1.5 Time-dependent Behavior

Only in an idealized, well equilibrated scenario is the operation of an SOC completely independent from temporal effects. On the one hand, operating conditions like voltage, current or gas composition can change in a short period of time, e.g., during startup or shutdown, inducing transient effects like temperature overshoots or momentary gas depletion. Such effects may then lead to amplified degradation and reduced lifetime. On the other hand, electrode properties like microstructure and composition can change over a prolonged period of operation due to degradation effects. This then may have an impact on the optimal operating strategy and also affects design choices of an SOC, since an optimal performance over the entire lifetime is the key target.

3.1.5.1 Transient Behavior

Models able to depict the dynamic response of an SOC due to changes in operating conditions comprise time-dependent formulations of the governing equations. This is especially important for those physical effects which characteristic time scale is in the range of the expected response time. Examination of the dynamic response to a given event often assumes a well-equilibrated steady state as starting point.

Several studies focus on the cell or stack response to rapid changes in the applied current [49, 56, 80, 183, 247–250].

Here [248, 249] are to highlight as they include both a high spatial and temporal resolution in a 3D channel RPU. To achieve this, only mass and heat transport are resolved in a time-dependent way and a quasi-stationary state for electrochemistry is assumed.

Further the response to temperature changes in startup operation [251–253] and for changing operation points [51] are investigated. [51, 254] also examines the influence of an operating voltage varying in time while [255] studies the time-dependent distribution of the chemical potential of oxygen through the cell.

3.1.5.2 Degradation

Over prolonged periods of operation, degradation can occur in several forms, as summarized for SOEC [256, 257] and SOFC [258]. As lifetime is a crucial point for commercialization of SOCs, the degradation of performance is modeled in various works.

For cermet fuel electrodes containing Nickel, microstructure changes over time due to Ni particle coarsening is a major issue. Larger Ni particles lead to a decrease in TPB density, percolation and thus performance. This is implemented via a time-dependent expression for the Ni particle radius or TPB [150, 151, 259–261] or by using the phase field method [48, 262]. Deactivation by chromium poisoning in LSM-YSZ oxygen electrodes is treated in a similar fashion adopting time dependent TPB lengths and chromium partial pressure dependent reaction rates [150, 151, 260, 261].

[245] implements an evolution equation for the long-term coarsening of Ni particles and deduces its effect on the conductivity of Ni-YSZ fuel electrode. A degradation induced change of the conductivity is also modeled in [260, 261] by applying a time law derived from fitting experimental data.

The formation of an oxide layer on the IC surface is described by an interfacial ASR that increases over time [151, 260, 261] or by introducing an additional potential drop [66]. A transient term for the thickness of the layer is divided by the conductivity of the oxide layer that determines the additional resistance.

The evolution of mechanical stress due to degradation is studied in [204, 213, 216] and the evolution of the failure probability with time is under consideration in [221–223].

In reformat operation, another ageing effect investigated is the deposition of carbon at the fuel electrode. Its impact on performance is studied in [263–265] consequences for the distribution of porosity and current density are shown in [263, 265].

Further detrimental effects examined are, for example, the accumulation of SrZrO₃ in the interlayer [266], formation of mixed phases on oxygen electrodes [260, 261] and sulfur poisoning during reformat operation [199].

3.2 Parametrization and Validation

The presented physical models comprising of mathematical equations rely on physical parameters to describe microstructural, geometrical, or material properties of the system under investigation. Parametrization often requires a high experimental effort and the use of advanced methods including:

- dynamic electrochemical analysis by means of impedance spectroscopy [40, 41, 184, 267–269]
 - tomography to obtain microstructural parameters of porous electrodes [112]
 - measurements of idealized model samples
 - gas analysis to evaluate electrochemical and catalytic gas conversion [79]
 - segmented testing approaches to evaluate gradients in larger size cells [55, 270–272]
- and many more.

As a result, authors sometimes resort to published data and parameters instead of conducting their own experiments. In this case, the conditions and assumptions under which the parameters were obtained should be examined carefully, so that a potential mismatch between how parameters are retrieved and utilized is avoided.

In order to check whether the model represents the actual system to a satisfying degree, a comparison of the two should be carried out. In the case of SOCs, such a validation is typically performed by comparison of simulated and measured CV curves [40, 41, 62, 91, 182, 184, 272] (Fig. 12). Characteristic of this form of validation is that the cumulative response of the entire cell or stack is evaluated. On the one hand, this means that the model should describe all relevant processes in a correct way in order to achieve meaningful results. On the other hand, since only the cumulative, averaged response is compared, the precise spatial distribution of certain fields and parameters cannot be validated by this method alone.

Measuring CV curves is not feasible for all research groups due to the costly experimental infrastructure needed.

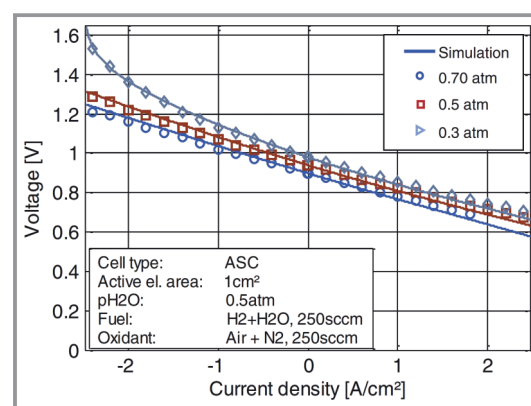


Figure 12. Simulation results of C/V curves at 800 °C in SOFC and SOEC operation modes for fuel electrode H₂O:H₂ compositions 70:30, 50:50 and 30:70 [41].

Hence, as for the parametrization data, most model developers resort to validation data from publicly available literature [51, 60, 85–87]. As mentioned before, experimental and cell parameters might be unknown or different from the own setup, which leads to uncertainties and sources of error in the validation.

Even if a study includes the determination of all relevant parameters using in-house experimental data, validation of the models by CV curves can be ambiguous. In order to reduce this risk and also to assure the agreement for the nonlinear parts of the CV curves, validation should be performed at multiple temperatures, gas compositions and up to high currents.

Additional to CV curves experimental evaluation of gas composition [79] or temperature [83] at multiple locations along the channel provides further information on the validity of the model. This is also the case for temporally resolved measurements of current density for transient models as presented for a 3D RPU in [248, 249].

4 Conclusion

Commercialization and large-scale application of SOE technology is speeding up significantly. Annual production capacities already reached the GW range enabling the deployment of systems in the MW scale. So far, they are mainly installed in the framework of demonstration projects providing hydrogen or syngas in various applications.

In order to improve and further develop SOECs, a thorough understanding of physical processes limiting performance and lifetime is required. Accessing and comprehending these processes by sole experimental methods, is often difficult and costly. This makes modeling a crucial asset for the development and continuous improvement of SOEC technology. In this review we have summarized various SOC models discussed in literature, differing in scope and scale. We hereto focus on the processes considered in the models and the approaches taken to implement them and give some recommendations on model features to be considered.

The studies reveal that the choice of processes to be considered in a model and their implementation depends on the aim of the study. Model geometry and resolution have to be chosen appropriately. Since computational capacities are limited, homogenization and simplifications cannot be avoided, but should be employed with care.

In general, the determination of required parameters specific to the modeled SOEC, such as, for example, material, microstructural and geometric parameters, is essential to correctly describe the actual behavior of the system. A model specific experimental parameterization workflow is required. Beyond parameterization, thorough experimental validation is vital to ensure trustworthy results before applying the developed model. Since own data for parametrization and validation is not always available, model developers have to resort to literature data, preferably from systems

similar to the ones modeled. In such cases, it is recommended to not only consider cell chemistry or concept, but also be aware of the operating conditions under which the experimental data was recorded.

Acknowledgment

Open access funding enabled and organized by Projekt DEAL.



Marius Müller studied chemical engineering at Karlsruhe Institute of Technology (KIT, Germany). In 2023 he started his PhD project on modeling of SOEC stacks at the Institute of Applied Materials – Electrochemical Technologies (IAM-ET) at KIT in collaboration with the corporate research division of Robert Bosch GmbH.



Markus Klinsmann studied physics at the University Stuttgart (Germany). He obtained his PhD degree in mechanical engineering at KIT Karlsruhe (Germany), in a collaboration with UC Santa Barbara (USA) and Robert Bosch GmbH. Since 2014, he works at Robert Bosch GmbH as a research engineer in the field of lithium ion and solid-state batteries, as well as fuel cells and electrolysis.



Ulrich Sauter studied chemical engineering at Karlsruhe Institute of Technology (Germany). He obtained his PhD degree (2005) in the field of fluid mechanics. In 2005 he started his career at Robert Bosch GmbH working in various expert and management roles in the field of electrochemical energy storage and conversion.

Currently, he is Chief Expert at Robert Bosch Corporate Research with responsibility for modeling and virtual engineering of electrochemical components, covering both low and high temperature fuel cells and electrolyzers.



Jean-Claude Njodzefon studied electrical engineering and information technology at the Karlsruhe Institute of Technology, KIT and obtained a PhD in chemical engineering at the Technical University of Denmark, DTU. Since 2016, he works as a Solid Oxide Cell expert and project leader at the corporate research of Robert Bosch GmbH.



André Weber is working as senior scientist and academic councilor at Karlsruhe Institute of Technology (see <http://www.iam.kit.edu/et/>). He is heading two groups at IAM-ET related to fuel cells & electrolysis and Li-batteries. The research focuses on electrochemical characterization and modeling of fuel cells, electrolyzers and

batteries, ranging from fundamental studies on model systems to the analysis of commercial products.

Abbreviations

AEL	alkaline electrolysis
AEM	anion exchange membrane electrolysis
ASR	area specific resistance
BFM	Binary Friction model
BV	Butler-Volmer
CV	current voltage
CPIM	cylindrical pore interpolation model
D	dimensional
DPB	double-phase-boundaries
DGM	dusty-gas model
EIS	electrochemical impedance spectroscopy
ESC	electrolyte supported cell
ECM	equivalent circuit model
FESC	fuel electrode supported cell
FM	Fick's model
FIB-SEM	focused ion beam – scanning electron microscope
GDC	gadolinium doped ceria
HT	high temperature
IC	interconnector
LSCF	$\text{La}_{1-x}\text{Sr}_x\text{Co}_{1-y}\text{Fe}_y\text{O}_{3-\delta}$
LSC	$\text{La}_{1-x}\text{Sr}_x\text{CoO}_{3-\delta}$
LSM	$\text{La}_{1-x}\text{Sr}_x\text{MnO}$
LTE	local thermal equilibrium
LT	low temperature
LHV	lower heating value
MSC	metal supported cell
MIEC	mixed ionic electronic conduction
NSE	Navier-Stokes equation
OESC	oxygen electrode supported cell
PEMEL	polymer membrane electrolysis
RPU	repeating unit
SDC	samarium doped ceria
ScSZ	scandia-, or scandia and ceria-stabilized zirconia
SOCs	solid oxide cells
SOE	Solid oxide electrolyzer
SOEC	solid oxide electrolysis cells
SOFC	solid oxide fuel cell
SMM	Stefan-Maxwell model
TEC	thermal expansion coefficients
TPB	three-phase-boundaries
TLM	transmission line model
YSZ	yttria-stabilized zirconia

References

- [1] H. Ghezal-Ayagh, *ECS Trans.* **2021**, *103* (1), 17–24. DOI: <https://doi.org/10.1149/10301.0017ecst>
- [2] Y. Pleshivtseva, M. Derevyanov, A. Pimenov, A. Rapoport, *Int. J. Hydrogen Energy* **2023**, *48*, 32191–32240. DOI: <https://doi.org/10.1016/j.ijhydene.2023.04.264>
- [3] A. Hauch, R. Küngas, P. Blennow, A. B. Hansen, J. B. Hansen, B. V. Mathiesen, M. B. Mogensen, *Science* **2020**, *370* (6513), eaba6118. DOI: <https://doi.org/10.1126/science.aba6118>

- [4] S. Shiva Kumar, H. Lim, *Energy Rep.* **2022**, *8*, 13793–13813. DOI: <https://doi.org/10.1016/j.egy.2022.10.127>
- [5] Ch. Neofytidis, E. Ioannidou, L. Sygellou, M. Kollia, D. K. Niakolas, *J. Catal.* **2019**, *373*, 260–275. DOI: <https://doi.org/10.1016/j.jcat.2019.04.002>
- [6] <https://www.topsoe.com/our-resources/knowledge/our-products/equipment/ecos-co-from-co2> (Accessed on August 25, 2023)
- [7] R. Küngas, P. Blennow, T. Heiredal-Clausen, T. Holt, J. Rass-Hansen, S. Primdahl, J. B. Hansen, *ECS Trans.* **2017**, *78* (1), 2879–2884. DOI: <https://doi.org/10.1149/07801.2879ecst>
- [8] <http://webbook.nist.gov/chemistry/> (Accessed on May 5, 2014)
- [9] S. D. Ebbesen, S. H. Jensen, A. Hauch, M. B. Mogensen, *Chem. Rev.* **2014**, *114* (21), 10697–10734. DOI: <https://doi.org/10.1021/cr5000865>
- [10] M. Noponen, P. Torri, J. Göös, J. Puranen, T. Lehtinen, S. Pylpko, E. Ounpuu, *ECS Trans.* **2021**, *103* (1), 267–274. DOI: <https://doi.org/10.1149/10301.0267ecst>
- [11] A. Hauch, P. G. Blennow, K. N. Dalby, D. B. Drasbæk, T. Heiredal-Clausen, A. K. Padinjarethil, G. Perin, J. Rass-Hansen, E. M. Sala, R. Tiruvalam, *ECS Trans.* **2023**, *111* (6), 1125–1133. DOI: <https://doi.org/10.1149/11106.1125ecst>
- [12] O. Posdziech, K. Schwarze, J. Brabandt, *Int. J. Hydrogen Energy* **2019**, *44* (35), 19089–19101. DOI: <https://doi.org/10.1016/j.ijhydene.2018.05.169>
- [13] G. Schiller, A. Ansar, M. Lang, O. Patz, *J. Appl. Electrochem.* **2009**, *39* (2), 293–301. DOI: <https://doi.org/10.1007/s10800-008-9672-6>
- [14] A. Hagen, R. Caldogno, F. Capotondo, X. Sun, *Energies* **2022**, *15* (6), 2045. DOI: <https://doi.org/10.3390/en15062045>
- [15] R. T. Leah, A. Bone, A. Selcuk, M. Rahman, A. Clare, M. Lankin, F. Felix, S. Mukerjee, M. Selby, *ECS Trans.* **2019**, *91* (1), 51–61. DOI: <https://doi.org/10.1149/09101.0051ecst>
- [16] R. Leah, A. Bone, A. Selcuk, M. Lankin, M. Rahman, A. Clare, G. Reade, F. Felix, J. De Vero, Xi. Wang, et al., *ECS Trans.* **2021**, *103* (1), 679–684. DOI: <https://doi.org/10.1149/10301.0679ecst>
- [17] E. Matte, G. Holzlechner, L. Epple, D. Stolten, P. Lupetin, *J. Power Sources* **2019**, *413*, 334–343. DOI: <https://doi.org/10.1016/j.jpowsour.2018.12.025>
- [18] F. Wankmüller, N. Russner, A. Weber, M. Meffert, J. Schmiege, H. Störmer, J.-C. Njodzefon, P. Lupetin, D. Gerthsen, E. Ivers-Tiffée, *ECS Trans.* **2019**, *91* (1), 501–509. DOI: <https://doi.org/10.1149/09101.0501ecst>
- [19] M. Fallah Vostakola, B. Amini Horri, *Energies* **2021**, *14* (5), 1280. DOI: <https://doi.org/10.3390/en14051280>
- [20] J. Schefold, A. Brisse, H. Poepke, *Electrochim. Acta* **2015**, *179*, 161–168. DOI: <https://doi.org/10.1016/j.electacta.2015.04.141>
- [21] D. Udomsilp, C. Lenser, O. Guillon, N. H. Menzler, *Energy Technol.* **2021**, *9* (4), 2001062. DOI: <https://doi.org/10.1002/ente.202001062>
- [22] S. Takahashi, H. Sumi, Y. Fujishiro, *ECS Trans.* **2019**, *91* (1), 571–577. DOI: <https://doi.org/10.1149/09101.0571ecst>
- [23] S. He, Y. Zou, K. Chen, S. P. Jiang, *Interdiscip. Mater.* **2023**, *2* (1), 111–136. DOI: <https://doi.org/10.1002/idm2.12068>
- [24] J. Mermelstein, M. Millan, N. Brandon, *J. Power Sources* **2010**, *195* (6), 1657–1666. DOI: <https://doi.org/10.1016/j.jpowsour.2009.09.046>
- [25] L. Zhang, S. P. Jiang, H. Q. He, X. Chen, J. Ma, X. C. Song, *Int. J. Hydrogen Energy* **2010**, *35* (22), 12359–12368. DOI: <https://doi.org/10.1016/j.ijhydene.2010.08.067>
- [26] C. M. Harrison, P. R. Slater, R. Steinberger-Wilkens, *Solid State Ionics* **2021**, *373*, 115799. DOI: <https://doi.org/10.1016/j.ssi.2021.115799>
- [27] R. Knibbe, J. Hjelm, M. Menon, N. Pryds, M. Søgaard, H. J. Wang, K. Neufeld, *J. Am. Ceram. Soc.* **2010**, *93* (9), 2877–2883. DOI: <https://doi.org/10.1111/j.1551-2916.2010.03763.x>
- [28] <https://salcos.salzgitter-ag.com/en/grinhy-20.html#c149623> (Accessed on August 24, 2023)
- [29] <https://www.sunfire.de/en/news/detail/renewable-hydrogen-project-multiplhy-worlds-largest-high-temperature-electrolyzer-from-sunfire-successfully-installed> (Accessed on August 24, 2023)
- [30] <https://www.ceres.tech/news/ceres-collaborates-with-bosch-and-linde-engineering-on-a-1mw-green-hydrogen-demonstration/> (Accessed on August 24, 2023)
- [31] <https://www.topsoe.com/press-releases/topsoe-and-first-ammonia> (Accessed on August 25, 2023)
- [32] <https://www.bloomenergy.com/bloomelectrolyzer/> (Accessed on August 30, 2023)
- [33] <https://www.bloomenergy.com/wp-content/uploads/bloom-energy-electrolyzer-datasheet-june-2023.pdf> (Accessed on August 30, 2023)
- [34] S. B. Beale, M. Andersson, C. Boigues-Muñoz, H. L. Frandsen, Z. Lin, S. J. McPhail, M. Ni, B. Sundén, A. Weber, A. Z. Weber, *Prog. Energy Combust. Sci.* **2021**, *85*, 100902. DOI: <https://doi.org/10.1016/j.pecs.2020.100902>
- [35] K. N. Grew, W. K. S. Chiu, *J. Power Sources* **2012**, *199*, 1–13. DOI: <https://doi.org/10.1016/j.jpowsour.2011.10.010>
- [36] M. Vogler, A. Bieberle-Hütter, L. Gauckler, J. Warnatz, W. G. Bessler, *J. Electrochem. Soc.* **2009**, *156* (5), B663. DOI: <https://doi.org/10.1149/1.3095477>
- [37] W. Bessler, J. Warnatz, D. Goodwin, *Solid State Ionics* **2007**, *177* (39–40), 3371–3383. DOI: <https://doi.org/10.1016/j.ssi.2006.10.020>
- [38] W. G. Bessler, M. Vogler, H. Störmer, D. Gerthsen, A. Utz, A. Weber, E. Ivers-Tiffée, *Phys. Chem. Chem. Phys.* **2010**, *12* (42), 13888. DOI: <https://doi.org/10.1039/c0cp00541j>
- [39] H. Zhu, R. J. Kee, V. M. Janardhanan, O. Deutschmann, D. G. Goodwin, *J. Electrochem. Soc.* **2005**, *152* (12), A2427. DOI: <https://doi.org/10.1149/1.2116607>
- [40] A. Leonide, Y. Apel, E. Ivers-Tiffée, *ECS Trans.* **2009**, *19* (20), 81–109. DOI: <https://doi.org/10.1149/1.3247567>
- [41] J.-C. Njodzefon, D. Klotz, A. Kromp, A. Weber, E. Ivers-Tiffée, *J. Electrochem. Soc.* **2013**, *160* (4), F313. DOI: <https://doi.org/10.1149/2.018304jes>
- [42] W. Y. Lee, D. Wee, A. F. Ghoniem, *J. Power Sources* **2009**, *186* (2), 417–427. DOI: <https://doi.org/10.1016/j.jpowsour.2008.10.009>
- [43] D. A. Noren, M. A. Hoffman, *J. Power Sources* **2005**, *152*, 175–181. DOI: <https://doi.org/10.1016/j.jpowsour.2005.03.174>
- [44] S. Campanari, P. Iora, *J. Power Sources* **2004**, *132* (1–2), 113–126. DOI: <https://doi.org/10.1016/j.jpowsour.2004.01.043>
- [45] A. V. Virkar, J. Chen, C. W. Tanner, J.-W. Kim, *Solid State Ionics* **2000**, *131* (1–2), 189–198. DOI: [https://doi.org/10.1016/S0167-2738\(00\)00633-0](https://doi.org/10.1016/S0167-2738(00)00633-0)
- [46] J. Udagawa, P. Aguiar, N. P. Brandon, *J. Power Sources* **2007**, *166* (1), 127–136. DOI: <https://doi.org/10.1016/j.jpowsour.2006.12.081>
- [47] M. Ni, M. K. H. Leung, D. Y. C. Leung, *Electrochim. Acta* **2007**, *52* (24), 6707–6718. DOI: <https://doi.org/10.1016/j.electacta.2007.04.084>
- [48] J. H. Kim, W. K. Liu, C. Lee, *Comput. Mech.* **2009**, *44* (5), 683–703. DOI: <https://doi.org/10.1007/s00466-009-0402-7>
- [49] Q. Cai, N. P. Brandon, C. S. Adjiman, *Front Energy Power Eng China* **2010**, *4* (2), 211–222. DOI: <https://doi.org/10.1007/s11708-010-0037-6>

- [50] V. Menon, V. M. Janardhanan, O. Deutschmann, *Chemical Engineering Science* **2014**, *110*, 83–93. DOI: <https://doi.org/10.1016/j.ces.2013.10.025>
- [51] K. Tseronis, I. Bonis, I. K. Kookos, C. Theodoropoulos, *Int. J. Hydrogen Energy* **2012**, *37* (1), 530–547. DOI: <https://doi.org/10.1016/j.ijhydene.2011.09.062>
- [52] S. Zeng, J. Parbey, G. Yu, M. Xu, T. Li, M. Andersson, *J. Power Sources* **2018**, *379*, 134–143. DOI: <https://doi.org/10.1016/j.jpowsour.2018.01.011>
- [53] W. Zhao, V. J. Pinfield, H. Wang, J. Xuan, Z. Niu, *Energy Convers. Manage.* **2023**, *280*, 116791. DOI: <https://doi.org/10.1016/j.enconman.2023.116791>
- [54] J. Laurencin, D. Kane, G. Delette, J. Deseure, F. Lefebvre-Joud, *J. Power Sources* **2011**, *196* (4), 2080–2093. DOI: <https://doi.org/10.1016/j.jpowsour.2010.09.054>
- [55] E. Da Rosa Silva, M. Hubert, B. Morel, H. Moussaoui, J. Debayle, J. Laurencin, *ECS Trans.* **2021**, *103* (1), 893–907. DOI: <https://doi.org/10.1149/10301.0893ecst>
- [56] L. van Biert, M. Godjevac, K. Visser, P. V. Aravind, *Appl. Energy* **2019**, *250*, 976–990. DOI: <https://doi.org/10.1016/j.apenergy.2019.05.053>
- [57] M. Andersson, H. Paradis, J. Yuan, B. Sundén, *Electrochim. Acta* **2013**, *109*, 881–893. DOI: <https://doi.org/10.1016/j.electacta.2013.08.018>
- [58] M. Andersson, J. Yuan, B. Sundén, *Int. J. Heat Mass Transfer* **2012**, *55* (4), 773–788. DOI: <https://doi.org/10.1016/j.ijheatmasstransfer.2011.10.032>
- [59] I. Khazaei, A. Rava, *Energy* **2017**, *119*, 235–244. DOI: <https://doi.org/10.1016/j.energy.2016.12.074>
- [60] M. García-Camprubí, S. Izquierdo, N. Fueyo, *Renewable Sustainable Energy Rev.* **2014**, *33*, 701–718. DOI: <https://doi.org/10.1016/j.rser.2014.02.034>
- [61] M. Mogensen, H. Frandsen, J. Nielsen, W. Li, T. Jacobsen, C. Graves, in *Proceedings of the Smart Energy Conversion and Storage Conference: IV Polish Forum, Krynica, Poland* **2013**.
- [62] M. Navasa, C. Graves, C. Chatzichristodoulou, T. Løye Skafte, B. Sundén, H. Lund Frandsen, *Int. J. Hydrogen Energy* **2018**, *43* (27), 11913–11931. DOI: <https://doi.org/10.1016/j.ijhydene.2018.04.164>
- [63] H.-C. Chang, G. Jaffé, *J. Chem. Phys.* **1952**, *20* (7), 1071–1077. DOI: <https://doi.org/10.1063/1.1700669>
- [64] A. Häffelin, J. Joos, M. Ender, A. Weber, E. Ivers-Tiffée, *J. Electrochem. Soc.* **2013**, *160* (8), F867. DOI: <https://doi.org/10.1149/2.093308jes>
- [65] M. Ni, *Int. J. Hydrogen Energy* **2012**, *37* (8), 6389–6399. DOI: <https://doi.org/10.1016/j.ijhydene.2012.01.072>
- [66] S. Yu, S. Zhang, D. Schäfer, R. Peters, F. Kunz, R.-A. Eichel, *Energies* **2023**, *16* (9), 3827. DOI: <https://doi.org/10.3390/en16093827>
- [67] E. Achenbach, *J. Power Sources* **1994**, *49* (1–3), 333–348. DOI: [https://doi.org/10.1016/0378-7753\(93\)01833-4](https://doi.org/10.1016/0378-7753(93)01833-4)
- [68] Y. M. Barzi, A. Raoufi, H. Lari, *Int. J. Hydrogen Energy* **2010**, *35* (17), 9468–9478. DOI: <https://doi.org/10.1016/j.ijhydene.2010.05.086>
- [69] Y. J. Kim, M. C. Lee, *Int. J. Hydrogen Energy* **2017**, *42* (29), 18504–18513. DOI: <https://doi.org/10.1016/j.ijhydene.2017.04.140>
- [70] Y. Xie, X. Xue, *Solid State Ionics* **2012**, *224*, 64–73. DOI: <https://doi.org/10.1016/j.ssi.2012.07.015>
- [71] Y. Xie, X. Xue, *J. Power Sources* **2012**, *209*, 81–89. DOI: <https://doi.org/10.1016/j.jpowsour.2012.02.077>
- [72] L. Maier, B. Schädle, K. Herrera Delgado, S. Tischer, O. Deutschmann, *Top. Catal.* **2011**, *54* (13–15), 845–858. DOI: <https://doi.org/10.1007/s11244-011-9702-1>
- [73] Y. Luo, Y. Shi, W. Li, M. Ni, N. Cai, *Int. J. Hydrogen Energy* **2014**, *39* (20), 10359–10373. DOI: <https://doi.org/10.1016/j.ijhydene.2014.05.018>
- [74] I. Zinovik, D. Poulidakos, *Electrochim. Acta* **2009**, *54* (26), 6234–6243. DOI: <https://doi.org/10.1016/j.electacta.2009.06.001>
- [75] J. Hanna, W. Y. Lee, Y. Shi, A. F. Ghoniem, *Prog. Energy Combust. Sci.* **2014**, *40*, 74–111. DOI: <https://doi.org/10.1016/j.pecs.2013.10.001>
- [76] A. Nakajo, Z. Wullemmin, P. Metzger, S. Diethelm, G. Schiller, D. Favrat et al., *J. Electrochem. Soc.* **2011**, *158* (9), B1083. DOI: <https://doi.org/10.1149/1.3596433>
- [77] H. Geisler, M. Kornely, A. Weber, E. Ivers-Tiffée, *ECS Trans.* **2013**, *57* (1), 2871–2881. DOI: <https://doi.org/10.1149/05701.2871ecst>
- [78] H. Geisler, A. Kromp, A. Weber, E. Ivers-Tiffée, *J. Electrochem. Soc.* **2014**, *161* (6), F778. DOI: <https://doi.org/10.1149/2.079406jes>
- [79] H. Geisler, S. Dierickx, A. Weber, E. Ivers-Tiffée, *ECS Trans.* **2015**, *68* (1), 2151–2158. DOI: <https://doi.org/10.1149/06801.2151ecst>
- [80] D. P. Xenos, P. Hofmann, K. D. Panopoulos, E. Kakaras, *Energy* **2015**, *81*, 84–102. DOI: <https://doi.org/10.1016/j.energy.2014.11.049>
- [81] A. Li, X. Fang, Z. Lin, *ECS Trans.* **2015**, *68* (1), 3025–3042. DOI: <https://doi.org/10.1149/06801.3025ecst>
- [82] A. Li, C. Song, Z. Lin, *Appl. Energy* **2017**, *190*, 1234–1244. DOI: <https://doi.org/10.1016/j.apenergy.2017.01.034>
- [83] N. Russner, S. Dierickx, A. Weber, R. Reimert, E. Ivers-Tiffée, *J. Power Sources* **2020**, *451*, 227552. DOI: <https://doi.org/10.1016/j.jpowsour.2019.227552>
- [84] C. Kang, P. Huaiwu, Z. Junfeng, X. Xinxin, Z. Shengchen, R. Jingxin, L. Biao, W. Yueshe, *Energy Sci. Eng.* **2022**, *10* (10), 3918–3927. DOI: <https://doi.org/10.1002/ese3.1255>
- [85] A. Banerjee, Y. Wang, J. Diercks, O. Deutschmann, *Appl. Energy* **2018**, *230*, 996–1013. DOI: <https://doi.org/10.1016/j.apenergy.2018.08.122>
- [86] D. H. Jeon, *Energy* **2019**, *188*, 116050. DOI: <https://doi.org/10.1016/j.energy.2019.11.6050>
- [87] A. Bertei, J. Mertens, C. Nicolella, *Electrochim. Acta* **2014**, *146*, 151–163. DOI: <https://doi.org/10.1016/j.electacta.2014.08.120>
- [88] J. Shi, X. Xue, *Electrochim. Acta* **2010**, *55* (18), 5263–5273. DOI: <https://doi.org/10.1016/j.electacta.2010.04.060>
- [89] D. H. Jeon, *Electrochim. Acta* **2009**, *54* (10), 2727–2736. DOI: <https://doi.org/10.1016/j.electacta.2008.11.048>
- [90] X. Jin, X. Xue, *Int. J. Hydrogen Energy* **2010**, *35* (14), 7321–7328. DOI: <https://doi.org/10.1016/j.ijhydene.2010.04.158>
- [91] S. Lee, H. Kim, K. J. Yoon, J.-W. Son, J.-H. Lee, B.-K. Kim, W. Choi, J. Hong, *Int. J. Heat Mass Transfer* **2016**, *97*, 77–93. DOI: <https://doi.org/10.1016/j.ijheatmasstransfer.2016.02.001>
- [92] Y. Shao, Y. Li, Z. Fu, J. Li, Q. Zhu, *Energies* **2023**, *16* (6), 2525. DOI: <https://doi.org/10.3390/en16062525>
- [93] G. Paasch, K. Micka, P. Gersdorf, *Electrochim. Acta* **1993**, *38* (18), 2653–2662. DOI: [https://doi.org/10.1016/0013-4686\(93\)85083-B](https://doi.org/10.1016/0013-4686(93)85083-B)
- [94] G. Paasch, *Electrochem. Commun.* **2000**, *2* (5), 371–375. DOI: [https://doi.org/10.1016/S1388-2481\(00\)00040-0](https://doi.org/10.1016/S1388-2481(00)00040-0)
- [95] V. Sonn, A. Leonide, E. Ivers-Tiffée, *J. Electrochem. Soc.* **2008**, *155* (7), B675. DOI: <https://doi.org/10.1149/1.2908860>
- [96] S. Dierickx, J. Joos, A. Weber, E. Ivers-Tiffée, *Electrochim. Acta* **2018**, *265*, 736–750. DOI: <https://doi.org/10.1016/j.electacta.2017.12.029>
- [97] S. Dierickx, T. Mundloch, A. Weber, E. Ivers-Tiffée, *J. Power Sources* **2019**, *415*, 69–82. DOI: <https://doi.org/10.1016/j.jpowsour.2019.01.043>

- [98] N. Russner, S. Dierickx, A. Weber, E. Ivers-Tiffée, in *Proc. of 14th European SOFC & SOE Forum (Eds: O. Bucheli, G. Geisser)*, EFCF, Lucerne Switzerland **2020**.
- [99] B. Rüger, A. Weber, E. Ivers-Tiffée, *ECS Trans.* **2007**, *7* (1), 2065–2074. DOI: <https://doi.org/10.1149/1.2729320>
- [100] B. Rüger, J. Joos, A. Weber, T. Carraro, E. Ivers-Tiffée, *ECS Trans.* **2009**, *25* (2), 1211–1220. DOI: <https://doi.org/10.1149/1.3205650>
- [101] T. Carraro, J. Joos, B. Rüger, A. Weber, E. Ivers-Tiffée, *Electrochim. Acta* **2012**, *77*, 315–323. DOI: <https://doi.org/10.1016/j.electacta.2012.04.109>
- [102] T. Carraro, J. Joos, B. Rüger, A. Weber, E. Ivers-Tiffée, *Electrochim. Acta* **2012**, *77*, 309–314. DOI: <https://doi.org/10.1016/j.electacta.2012.04.163>
- [103] E. Effori, J. Laurencin, E. D. R. Silva, M. Hubert, T. David, M. Petitjean, G. Geneste, L. Dessemond, E. Siebert, *J. Electrochem. Soc.* **2021**, *168* (4), 044520. DOI: <https://doi.org/10.1149/1945-7111/abf40a>
- [104] A. Häffelin, C. Niedrig, S. F. Wagner, S. Baumann, W. A. Meulenber, E. Ivers-Tiffée, *J. Electrochem. Soc.* **2014**, *161* (14), F1409. DOI: <https://doi.org/10.1149/2.0601414jes>
- [105] J. Szász, F. Wankmüller, J. Joos, V. Wilde, H. Störmer, D. Gerthsen, E. Ivers-Tiffée, *ECS Trans.* **2017**, *77* (10), 27–34. DOI: <https://doi.org/10.1149/07710.0027ecst>
- [106] K. Cook, J. Wrubel, Z. Ma, K. Huang, X. Jin, *J. Electrochem. Soc.* **2021**, *168* (11), 114510. DOI: <https://doi.org/10.1149/1945-7111/ac35fc>
- [107] S. Panisset, M. Burriel, J. Laurencin, D. Jauffres, *J. Phys. Energy* **2023**, *5* (2), 022003. DOI: <https://doi.org/10.1088/2515-7655/acc5b1>
- [108] M. Ni, M. K. H. Leung, D. Y. C. Leung, *J. Power Sources* **2007**, *168* (2), 369–378. DOI: <https://doi.org/10.1016/j.jpowsour.2007.03.005>
- [109] S. Liu, W. Kong, Z. Lin, *Energies* **2009**, *2* (2), 427–444. DOI: <https://doi.org/10.3390/en20200427>
- [110] D. Chen, W. Bi, W. Kong, Z. Lin, *J. Power Sources* **2010**, *195* (19), 6598–6610. DOI: <https://doi.org/10.1016/j.jpowsour.2010.04.065>
- [111] A. N. Celik, *Int. J. Hydrogen Energy* **2018**, *43* (42), 19730–19748. DOI: <https://doi.org/10.1016/j.ijhydene.2018.08.212>
- [112] J. Joos, T. Carraro, A. Weber, E. Ivers-Tiffée, *J. Power Sources* **2011**, *196* (17), 7302–7307. DOI: <https://doi.org/10.1016/j.jpowsour.2010.10.006>
- [113] J. Joos, *Microstructural Characterisation, Modelling and Simulation of Solid Oxide Fuel Cell Cathodes*, KIT Scientific Publishing, Karlsruhe **2017**.
- [114] J. W. Essam, *Rep. Prog. Phys.* **1980**, *43* (7), 833. DOI: <https://doi.org/10.1088/0034-4885/43/7/001>
- [115] K. Zheng, L. Li, M. Ni, *Int. J. Hydrogen Energy* **2014**, *39* (24), 12904–12912. DOI: <https://doi.org/10.1016/j.ijhydene.2014.06.108>
- [116] D. Chen, Z. Lin, H. Zhu, R. J. Kee, *J. Power Sources* **2009**, *191* (2), 240–252. DOI: <https://doi.org/10.1016/j.jpowsour.2009.02.051>
- [117] V. M. Janardhanan, O. Deutschmann, *Electrochim. Acta* **2011**, *56* (27), 9775–9782. DOI: <https://doi.org/10.1016/j.electacta.2011.08.038>
- [118] B. Völker, R. M. McMeeking, *J. Power Sources* **2012**, *215*, 199–215. DOI: <https://doi.org/10.1016/j.jpowsour.2012.05.014>
- [119] P. Costamagna, P. Costa, V. Antonucci, *Electrochim. Acta* **1998**, *43* (3–4), 375–394. DOI: [https://doi.org/10.1016/S0013-4686\(97\)00063-7](https://doi.org/10.1016/S0013-4686(97)00063-7)
- [120] A. Bertei, C. Nicoletta, *J. Power Sources* **2011**, *196* (22), 9429–9436. DOI: <https://doi.org/10.1016/j.jpowsour.2011.06.087>
- [121] M. Chen, Z. Lin, *Int. J. Hydrogen Energy* **2014**, *39* (28), 15982–15988. DOI: <https://doi.org/10.1016/j.ijhydene.2014.01.081>
- [122] Z. Fu, Z. Wang, Y. Li, J. Li, Y. Shao, Q. Zhu, P. Weng, *Energies* **2022**, *15* (19), 7173. DOI: <https://doi.org/10.3390/en15197173>
- [123] S. Toros, *Ceram. Int.* **2016**, *42* (7), 8915–8924. DOI: <https://doi.org/10.1016/j.ceramint.2016.02.148>
- [124] M. Neumann, J. Staněk, O. M. Pecho, L. Holzer, V. Beneš, V. Schmidt, *Comput. Mater. Sci.* **2016**, *118*, 353–364. DOI: <https://doi.org/10.1016/j.commatsci.2016.03.013>
- [125] H. Moussaoui, J. Laurencin, Y. Gavet, G. Delette, M. Hubert, P. Cloetens, T. Le Bihan, J. Debayle, *Comput. Mater. Sci.* **2018**, *143*, 262–276. DOI: <https://doi.org/10.1016/j.commatsci.2017.11.015>
- [126] H. Moussaoui, J. Debayle, Y. Gavet, P. Cloetens, J. Laurencin, *Powder Technol.* **2020**, *367*, 67–81. DOI: <https://doi.org/10.1016/j.powtec.2020.03.040>
- [127] K. Zheng, Y. Zhang, L. Li, M. Ni, *Int. J. Hydrogen Energy* **2015**, *40* (1), 665–669. DOI: <https://doi.org/10.1016/j.ijhydene.2014.10.111>
- [128] G. Reiss, H. L. Frandsen, W. Brandstätter, A. Weber, *J. Power Sources* **2015**, *273*, 1006–1015. DOI: <https://doi.org/10.1016/j.jpowsour.2014.09.185>
- [129] W. Li, Y. Shi, Y. Luo, N. Cai, *Int. J. Hydrogen Energy* **2014**, *39* (25), 13738–13750. DOI: <https://doi.org/10.1016/j.ijhydene.2014.03.014>
- [130] Z. Zhou, L. Xing, V. Venkatesan, H. Xu, W. Chen, J. Xuan, *Fuel Cells* **2023**, *23* (1), 119–134. DOI: <https://doi.org/10.1002/fuce.202200151>
- [131] A. Abbaspour, K. Nandakumar, J. Luo, K. T. Chuang, *J. Power Sources* **2006**, *161* (2), 965–970. DOI: <https://doi.org/10.1016/j.jpowsour.2006.05.021>
- [132] M. Guo, Q. He, C. Cheng, D. Zhao, M. Ni, *J. Power Sources* **2022**, *533*, 231373. DOI: <https://doi.org/10.1016/j.jpowsour.2022.231373>
- [133] W. G. Bessler, S. Gewies, *J. Electrochem. Soc.* **2007**, *154* (6), B548. DOI: <https://doi.org/10.1149/1.2720639>
- [134] V. Menon, V. M. Janardhanan, S. Tischer, O. Deutschmann, *J. Power Sources* **2012**, *214*, 227–238. DOI: <https://doi.org/10.1016/j.jpowsour.2012.03.114>
- [135] L. Wehrle, D. Schmider, J. Dailly, A. Banerjee, O. Deutschmann, *Appl. Energy* **2022**, *317*, 119143. DOI: <https://doi.org/10.1016/j.apenergy.2022.119143>
- [136] K. Tseronis, I. K. Kookos, C. Theodoropoulos, *Chem. Eng. Sci.* **2008**, *63* (23), 5626–5638. DOI: <https://doi.org/10.1016/j.ces.2008.07.037>
- [137] S. B. Beale, H.-W. Choi, J. G. Pharoah, H. K. Roth, H. Jasak, D. H. Jeon, *Comput. Phys. Commun.* **2016**, *200*, 15–26. DOI: <https://doi.org/10.1016/j.cpc.2015.10.007>
- [138] M. Ni, *Int. J. Hydrogen Energy* **2009**, *34* (18), 7795–7806. DOI: <https://doi.org/10.1016/j.ijhydene.2009.07.080>
- [139] R. T. Nishida, S. B. Beale, J. G. Pharoah, *Int. J. Hydrogen Energy* **2016**, *41* (45), 20592–20605. DOI: <https://doi.org/10.1016/j.ijhydene.2016.05.103>
- [140] H.-W. Choi, J. G. Pharoah, D. Ryland, A. Kettner, N. Gnanapragasam, *ECS Trans.* **2013**, *57* (1), 3161–3170. DOI: <https://doi.org/10.1149/05701.3161ecst>
- [141] V. M. Janardhanan, O. Deutschmann, *J. Power Sources* **2006**, *162* (2), 1192–1202. DOI: <https://doi.org/10.1016/j.jpowsour.2006.08.017>
- [142] M. Nerat, Đ. Juričić, *Int. J. Hydrogen Energy* **2016**, *41* (5), 3613–3627. DOI: <https://doi.org/10.1016/j.ijhydene.2015.11.136>
- [143] M. Navasa, J. Yuan, B. Sundén, *Appl. Energy* **2015**, *137*, 867–876. DOI: <https://doi.org/10.1016/j.apenergy.2014.04.104>
- [144] M. Guo, X. Ru, L. Yang, M. Ni, Z. Lin, *Appl. Energy* **2022**, *322*, 119464. DOI: <https://doi.org/10.1016/j.apenergy.2022.119464>

- [145] T. Cui, G. Xiao, H. Yan, Y. Zhang, J.-Q. Wang, *Int. J. Green Energy* **2023**, *20* (4), 432–444. DOI: <https://doi.org/10.1080/15435075.2022.2065881>
- [146] S. Liu, C. Song, Z. Lin, *J. Power Sources* **2008**, *183* (1), 214–225. DOI: <https://doi.org/10.1016/j.jpowsour.2008.04.054>
- [147] S. Liu, W. Kong, Z. Lin, *J. Power Sources* **2009**, *194* (2), 854–863. DOI: <https://doi.org/10.1016/j.jpowsour.2009.06.056>
- [148] K. Daneshvar, G. Dotelli, C. Cristiani, R. Pelosato, M. Santarelli, *Fuel Cells* **2014**, *14* (2), 189–199. DOI: <https://doi.org/10.1002/fuce.201300235>
- [149] S. Lee, H. Kim, K. J. Yoon, J.-W. Son, J.-H. Lee, B.-K. Kim, W. Choi, J. Hong, *TEST* **2016**, *97*, 77–93. DOI: <https://doi.org/10.1016/j.ijheatmasstransfer.2016.02.001>
- [150] B. Bosio, F. R. Bianchi, *Sustainable Energy Fuels* **2023**, *7* (1), 280–293. DOI: <https://doi.org/10.1039/D2SE01118B>
- [151] O. B. Rizvandi, X.-Y. Miao, H. L. Frandsen, *Int. J. Hydrogen Energy* **2021**, *46* (54), 27709–27730. DOI: <https://doi.org/10.1016/j.ijhydene.2021.05.204>
- [152] J. Laurencin, F. Lefebvre-Joud, G. Delette, *J. Power Sources* **2008**, *177* (2), 355–368. DOI: <https://doi.org/10.1016/j.jpowsour.2007.11.099>
- [153] K. Sudaprasert, R. P. Travis, R. F. Martinez-Botas, *J. Fuel Cell Sci. Technol.* **2010**, *7* (1), 011002. DOI: <https://doi.org/10.1115/1.3080810>
- [154] D. F. Fairbanks, C. R. Wilke, *Ind. Eng. Chem.* **1950**, *42* (3), 471–475. DOI: <https://doi.org/10.1021/ie50483a022>
- [155] A. V. Akkaya, *Int. J. Energy Res.* **2007**, *31* (1), 79–98. DOI: <https://doi.org/10.1002/er.1238>
- [156] D. W. Reid, K. L. Teo, *Int. J. Syst. Sci.* **1977**, *8* (5), 497–511. DOI: <https://doi.org/10.1080/00207727708942059>
- [157] Y. Vural, L. Ma, D. B. Ingham, M. Pourkashanian, *J. Power Sources* **2010**, *195* (15), 4893–4904. DOI: <https://doi.org/10.1016/j.jpowsour.2010.01.033>
- [158] A. Bertei, C. Nicoletta, *J. Power Sources* **2015**, *279*, 133–137. DOI: <https://doi.org/10.1016/j.jpowsour.2015.01.007>
- [159] G. F. Froment, J. De Wilde, K. B. Bischoff, *Chemical Reactor Analysis and Design*, 3rd ed ed., Wiley, Hoboken, NJ, **2011**.
- [160] R. Krishna, J. A. Wesselingh, *Chem. Eng. Sci.* **1997**, *52* (6), 861–911. DOI: [https://doi.org/10.1016/S0009-2509\(96\)00458-7](https://doi.org/10.1016/S0009-2509(96)00458-7)
- [161] C. F. Curtiss, R. B. Bird, *Ind. Eng. Chem. Res.* **1999**, *38* (7), 2515–2522. DOI: <https://doi.org/10.1021/ie9901123>
- [162] E. A. Mason, A. P. Malinauskas, *Chem. Eng. Monogr.* **1983**, *17*, 161–174. DOI: <https://doi.org/10.1063/1.1841191>
- [163] S. K. Das, *Chem. Eng. Sci.* **2019**, *203*, 293–301. DOI: <https://doi.org/10.1016/j.ces.2019.03.085>
- [164] W. Kong, H. Zhu, Z. Fei, Z. Lin, *J. Power Sources* **2012**, *206*, 171–178. DOI: <https://doi.org/10.1016/j.jpowsour.2012.01.107>
- [165] P. J. Kerkhof, *Chem. Eng. J. Biochem. Eng. J.* **1996**, *64* (3), 319–343. DOI: [https://doi.org/10.1016/S0923-0467\(96\)03134-X](https://doi.org/10.1016/S0923-0467(96)03134-X)
- [166] J. B. Young, B. Todd, *Int. J. Heat Mass Transfer* **2005**, *48* (25–26), 5338–5353. DOI: <https://doi.org/10.1016/j.ijheatmasstransfer.2005.07.034>
- [167] W. Kast, C.-R. Hohenthanner, *Int. J. Heat Mass Transfer* **2000**, *43* (5), 807–823. DOI: [https://doi.org/10.1016/S0017-9310\(99\)00158-1](https://doi.org/10.1016/S0017-9310(99)00158-1)
- [168] S. Wang, W. M. Worek, W. J. Minkowycz, *Int. J. Heat Mass Transfer* **2012**, *55* (15–16), 3933–3945. DOI: <https://doi.org/10.1016/j.ijheatmasstransfer.2012.03.024>
- [169] R. Suwanwarangkul, E. Croiset, M. W. Fowler, P. L. Douglas, E. Entchev, M. A. Douglas, *J. Power Sources* **2003**, *122* (1), 9–18. DOI: [https://doi.org/10.1016/S0378-7753\(02\)00724-3](https://doi.org/10.1016/S0378-7753(02)00724-3)
- [170] Y. Fu, Y. Jiang, S. Poizeau, A. Dutta, A. Mohanram, J. D. Pietras, M. Z. Bazant, *J. Electrochem. Soc.* **2015**, *162* (6), F613. DOI: <https://doi.org/10.1149/2.0911506jes>
- [171] M. Blesznowski, M. Sikora, J. Kupecki, L. Makowski, W. Orciuch, *Energy* **2022**, *239*, 121878. DOI: <https://doi.org/10.1016/j.energy.2021.121878>
- [172] Y. Shi, N. Cai, C. Li, *J. Power Sources* **2007**, *164* (2), 639–648. DOI: <https://doi.org/10.1016/j.jpowsour.2006.10.091>
- [173] E. N. Fuller, P. D. Schettler, J. Calvin. Giddings, *Ind. Eng. Chem.* **1966**, *58* (5), 18–27. DOI: <https://doi.org/10.1021/ie50677a007>
- [174] B. E. Poling, J. M. Prausnitz, J. P. O'Connell, *The Properties of Gases and Liquids*, 5th ed., McGraw-Hill, New York **2001**.
- [175] S. Chapman, T. G. Cowling, *The Mathematical Theory of Non-Uniform Gases: An Account of the Kinetic Theory of Viscosity, Thermal Conduction, and Diffusion in Gases*, 3rd ed., Cambridge University Press, Cambridge, New York **1990**.
- [176] E. L. Cussler, *Diffusion: Mass Transfer in Fluid Systems*, 3rd ed., Cambridge University Press, Cambridge, New York **2009**.
- [177] W. G. Bessler, S. Gewies, M. Vogler, *Electrochim. Acta* **2007**, *53* (4), 1782–1800. DOI: <https://doi.org/10.1016/j.electacta.2007.08.030>
- [178] M. Navasa, X.-Y. Miao, H. L. Frandsen, *Int. J. Hydrog. Energy* **2019**, *44* (41), 23330–23347. DOI: <https://doi.org/10.1016/j.ijhydene.2019.06.077>
- [179] C. Jiang, Y. Gu, W. Guan, J. Zheng, M. Ni, Z. Zhong, *Int. J. Hydrogen Energy* **2020**, *45* (1), 904–915. DOI: <https://doi.org/10.1016/j.ijhydene.2019.10.139>
- [180] A. Weber, H. Geisler, *ECS Trans.* **2019**, *91* (1), 2233–2240. DOI: <https://doi.org/10.1149/09101.2233ecst>
- [181] L. Wehrle, Y. Wang, P. Boldrin, N. P. Brandon, O. Deutschmann, A. Banerjee, *ACS Environ. Au.* **2022**, *2* (1), 42–64. DOI: <https://doi.org/10.1021/acsenvironau.1c00014>
- [182] J. S. Herring, J. E. O'Brien, C. M. Stoots, G. L. Hawkes, J. J. Hartvigsen, M. Shahnam, *Int. J. Hydrogen Energy* **2007**, *32* (4), 440–450. DOI: <https://doi.org/10.1016/j.ijhydene.2006.06.061>
- [183] G. Botta, M. Romeo, A. Fernandes, S. Trabucchi, P. V. Aravind, *Energy Convers. Manage.* **2019**, *185*, 636–653. DOI: <https://doi.org/10.1016/j.enconman.2019.01.082>
- [184] A. Leonide, S. Hansmann, A. Weber, E. Ivers-Tiffée, *J. Power Sources* **2011**, *196* (17), 7343–7346. DOI: <https://doi.org/10.1016/j.jpowsour.2010.10.052>
- [185] D. Klotz, J. P. Schmidt, A. Weber, E. Ivers-Tiffée, *J. Power Sources* **2014**, *259*, 65–75. DOI: <https://doi.org/10.1016/j.jpowsour.2014.02.028>
- [186] D. Klotz, A. Leonide, A. Weber, E. Ivers-Tiffée, *Int. J. Hydrogen Energy* **2014**, *39* (35), 20844–20849. DOI: <https://doi.org/10.1016/j.ijhydene.2014.08.139>
- [187] J. Udagawa, P. Aguiar, N. P. Brandon, *J. Power Sources* **2008**, *180* (1), 46–55. DOI: <https://doi.org/10.1016/j.jpowsour.2008.02.026>
- [188] M. Ni, *Chem. Eng. J.* **2010**, *164* (1), 246–254. DOI: <https://doi.org/10.1016/j.cej.2010.08.032>
- [189] Y. Shi, Y. Luo, N. Cai, J. Qian, S. Wang, W. Li, H. Wang, *Electrochim. Acta* **2013**, *88*, 644–653. DOI: <https://doi.org/10.1016/j.electacta.2012.10.107>
- [190] G. M. Goldin, H. Zhu, R. J. Kee, D. Bierschen, S. A. Barnett, *J. Power Sources* **2009**, *187* (1), 123–135. DOI: <https://doi.org/10.1016/j.jpowsour.2008.10.097>
- [191] M. Peksens, *Int. J. Hydrogen Energy* **2011**, *36* (18), 11914–11928. DOI: <https://doi.org/10.1016/j.ijhydene.2011.06.045>
- [192] D. H. Kim, Y. Bae, S. Lee, J.-W. Son, J. H. Shim, J. Hong, *Energy Convers. Manage.* **2020**, *222*, 113213. DOI: <https://doi.org/10.1016/j.enconman.2020.113213>
- [193] P. Pianko-Oprych, T. Zinko, Z. Jaworski, *Materials* **2016**, *9* (10), 814. DOI: <https://doi.org/10.3390/ma9100814>
- [194] K. Zheng, Q. Sun, M. Ni, *Energy Technol.* **2013**, *1* (1), 35–41. DOI: <https://doi.org/10.1002/ente.201200014>

- [195] S. Lee, M. Park, H. Kim, K. J. Yoon, J.-W. Son, J.-H. Lee, B.-K. Kim, W. Choi, J. Hong, *Energy* **2017**, *120*, 293–305. DOI: <https://doi.org/10.1016/j.energy.2016.11.084>
- [196] M. Zeng, J. Yuan, J. Zhang, B. Sundén, Q. Wang, *J. Power Sources* **2012**, *206*, 185–196. DOI: <https://doi.org/10.1016/j.jpowsour.2012.01.130>
- [197] D. L. Damm, A. G. Fedorov, *J. Power Sources* **2005**, *143* (1–2), 158–165. DOI: <https://doi.org/10.1016/j.jpowsour.2004.11.063>
- [198] D. Sánchez, R. Chacartegui, A. Muñoz, T. Sánchez, *J. Power Sources* **2006**, *160* (2), 1074–1087. DOI: <https://doi.org/10.1016/j.jpowsour.2006.02.098>
- [199] N. Russner, H. Geisler, S. Dierickx, A. Weber, E. Ivers-Tiffée, *ECS Trans.* **2017**, *78* (1), 2673–2682. DOI: <https://doi.org/10.1149/07801.2673ecst>
- [200] C. Bao, N. Cai, E. Croiset, *J. Power Sources* **2011**, *196* (6), 3223–3232. DOI: <https://doi.org/10.1016/j.jpowsour.2010.11.128>
- [201] R. T. Nishida, S. B. Beale, J. G. Pharoah, L. G. J. de Haart, L. Blum, *J. Power Sources* **2018**, *373*, 203–210. DOI: <https://doi.org/10.1016/j.jpowsour.2017.10.030>
- [202] J. Ma, S. Ma, X. Zhang, D. Chen, J. He, *Sustainability* **2018**, *10* (9), 3094. DOI: <https://doi.org/10.3390/su10093094>
- [203] W. C. Tan, E. A. Lim, H. Abd Rahman, A. Abdul Samat, C. S. Oon, *Int. J. Hydrogen Energy* **2023**, *48* (50), 19217–19232. DOI: <https://doi.org/10.1016/j.ijhydene.2023.01.361>
- [204] M. Peksen, *Int. J. Hydrogen Energy* **2013**, *38* (30), 13408–13418. DOI: <https://doi.org/10.1016/j.ijhydene.2013.07.112>
- [205] M. Peksen, A. Al-Masri, L. Blum, D. Stolten, *Int. J. Hydrogen Energy* **2013**, *38* (10), 4099–4107. DOI: <https://doi.org/10.1016/j.ijhydene.2013.01.072>
- [206] H. I. Geisler, *Finite Element Method (FEM) Model and Performance Analysis of Solid Oxide Fuel Cells*, Vol. 36, KIT Scientific Publishing **2019**.
- [207] S. Lee, Y. Bae, K. J. Yoon, J.-H. Lee, W. Choi, J. Hong, *Energy Convers. Manage.* **2018**, *174*, 565–578. DOI: <https://doi.org/10.1016/j.enconman.2018.08.064>
- [208] E. Achenbach, *ECS Proc. Vol.* **1995**, *1995-1* (1), 1095–1104. DOI: <https://doi.org/10.1149/199501.1095PV>
- [209] G. Hawkes, J. O'Brien, C. Stoots, B. Hawkes, *Int. J. Hydrogen Energy* **2009**, *34* (9), 4189–4197. DOI: <https://doi.org/10.1016/j.ijhydene.2008.11.068>
- [210] C. Wang, J. Jun Yang, W. Huang, T. Zhang, D. Yan, J. Pu, B. Chi, J. Li, *Int. J. Hydrogen Energy* **2018**, *43* (45), 20900–20910. DOI: <https://doi.org/10.1016/j.ijhydene.2018.08.076>
- [211] E. Guk, M. Ranaweera, V. Venkatesan, J.-S. Kim, W. Jung, *Appl. Energy* **2020**, *280*, 116013. DOI: <https://doi.org/10.1016/j.apenergy.2020.116013>
- [212] M. A. S. Zaghoul, J. H. Mason, M. Wang, M. Buric, Z. Peng, S. Lee, P. Ohodnicki, H. Abernathy, K. P. Chen, *Appl. Energy* **2021**, *288*, 116633. DOI: <https://doi.org/10.1016/j.apenergy.2021.116633>
- [213] T. T. Molla, K. Kwok, H. L. Frandsen, *Fuel Cells* **2019**, *19* (1), 96–109. DOI: <https://doi.org/10.1002/fuce.201800081>
- [214] S.-S. Wei, T.-H. Wang, J.-S. Wu, *Energy* **2014**, *69*, 553–561. DOI: <https://doi.org/10.1016/j.energy.2014.03.052>
- [215] G. Kaur, D. Homa, K. Singh, O. P. Pandey, B. Scott, G. Pickrell, *J. Power Sources* **2013**, *242*, 305–313. DOI: <https://doi.org/10.1016/j.jpowsour.2013.05.094>
- [216] A. Nakajo, J. Van herle, D. Favrat, *Fuel Cells* **2011**, *11* (4), 537–552. DOI: <https://doi.org/10.1002/fuce.201000108>
- [217] K. Kwok, D. Boccaccini, Å. H. Persson, H. L. Frandsen, *Int. J. Solids Struct.* **2016**, *78–79*, 38–46. DOI: <https://doi.org/10.1016/j.ijsolstr.2015.09.020>
- [218] S. Celik, B. Ibrahimoglu, M. D. Mat, Y. Kaplan, T. N. Veziroglu, *Int. J. Hydrogen Energy* **2015**, *40* (24), 7895–7902. DOI: <https://doi.org/10.1016/j.ijhydene.2014.10.057>
- [219] W. A. Weibull, *IVB-Handl.* **1939**.
- [220] A. Nakajo, Z. Wuillemin, J. Van herle, D. Favrat, *J. Power Sources* **2009**, *193* (1), 203–215. DOI: <https://doi.org/10.1016/j.jpowsour.2008.12.050>
- [221] A. Nakajo, F. Mueller, J. Brouwer, J. Van herle, D. Favrat, *Int. J. Hydrogen Energy* **2012**, *37* (11), 9249–9268. DOI: <https://doi.org/10.1016/j.ijhydene.2012.03.043>
- [222] A. Nakajo, F. Mueller, J. Brouwer, J. Van herle, D. Favrat, *Int. J. Hydrogen Energy* **2012**, *37* (11), 9269–9286. DOI: <https://doi.org/10.1016/j.ijhydene.2012.03.023>
- [223] F. Greco, H. L. Frandsen, A. Nakajo, M. F. Madsen, J. Van herle, *J. Eur. Ceram. Soc.* **2014**, *34* (11), 2695–2704. DOI: <https://doi.org/10.1016/j.jeurceramsoc.2013.12.055>
- [224] J. Bao, N. Karri, K. Recknagle, C. Wang, B. Koeppel, O. A. Marina, *J. Electrochem. Soc.* **2022**, *169* (5), 054523. DOI: <https://doi.org/10.1149/1945-7111/ac6f87>
- [225] B. N. Nguyen, N. K. Karri, C. T. Mason, J. F. Fitzpatrick, B. J. Koeppel, *J. Electrochem. Soc.* **2021**, *168* (11), 114514. DOI: <https://doi.org/10.1149/1945-7111/ac39de>
- [226] X.-Y. Miao, O. B. Rizvandi, M. Navasa, H. L. Frandsen, *Appl. Energy* **2021**, *293*, 116901. DOI: <https://doi.org/10.1016/j.apenergy.2021.116901>
- [227] A. Nakajo, Z. Wuillemin, J. Van herle, D. Favrat, *J. Power Sources* **2009**, *193* (1), 216–226. DOI: <https://doi.org/10.1016/j.jpowsour.2008.12.039>
- [228] J. I. Gazzarri, O. Kesler, *J. Power Sources* **2008**, *176* (1), 138–154. DOI: <https://doi.org/10.1016/j.jpowsour.2007.10.047>
- [229] M. Nerat, D. Juričić, *Int. J. Hydrogen Energy* **2018**, *43* (17), 8179–8189. DOI: <https://doi.org/10.1016/j.ijhydene.2018.02.189>
- [230] M. Kornely, A. Leonide, A. Weber, E. Ivers-Tiffée, *ECS Trans.* **2009**, *25* (2), 815–824. DOI: <https://doi.org/10.1149/1.3205600>
- [231] M. Kornely, A. Leonide, A. Weber, E. Ivers-Tiffée, *J. Power Sources* **2011**, *196* (17), 7209–7216. DOI: <https://doi.org/10.1016/j.jpowsour.2010.10.048>
- [232] W. Kong, J. Li, S. Liu, Z. Lin, *J. Power Sources* **2012**, *204*, 106–115. DOI: <https://doi.org/10.1016/j.jpowsour.2012.01.041>
- [233] C. W. Tanner, A. V. Virkar, *J. Power Sources* **2003**, *113*, 44–56. DOI: [https://doi.org/10.1016/S0378-7753\(02\)00479-2](https://doi.org/10.1016/S0378-7753(02)00479-2)
- [234] Q. Chen, M. Zeng, J. Zhang, Q. Wang, *Int. J. Hydrogen Energy* **2010**, *35* (9), 4292–4300. DOI: <https://doi.org/10.1016/j.ijhydene.2010.01.117>
- [235] Y. Wang, Y. Du, M. Ni, R. Zhan, Q. Du, K. Jiao, *Appl. Therm. Eng.* **2020**, *172*, 114959. DOI: <https://doi.org/10.1016/j.applthermaleng.2020.114959>
- [236] W. Bi, J. Li, Z. Lin, *J. Power Sources* **2010**, *195* (10), 3207–3214. DOI: <https://doi.org/10.1016/j.jpowsour.2009.11.127>
- [237] D. Chen, Q. Zeng, S. Su, W. Bi, Z. Ren, *Appl. Energy* **2013**, *112*, 1100–1107. DOI: <https://doi.org/10.1016/j.apenergy.2013.04.035>
- [238] K. Rashid, S. K. Dong, R. A. Khan, S. H. Park, *J. Power Sources* **2016**, *327*, 638–652. DOI: <https://doi.org/10.1016/j.jpowsour.2016.07.077>
- [239] C. Zhao, J. Yang, T. Zhang, D. Yan, J. Pu, B. Chi, J. Li, *Int. J. Hydrogen Energy* **2020**, *45* (28), 14440–14451. DOI: <https://doi.org/10.1016/j.ijhydene.2020.02.143>
- [240] W. C. Tan, H. Iwai, M. Kishimoto, H. Yoshida, *J. Power Sources* **2018**, *400*, 135–146. DOI: <https://doi.org/10.1016/j.jpowsour.2018.08.002>
- [241] M. Roos, E. Batawi, U. Harnisch, Th. Hocker, *J. Power Sources* **2003**, *118* (1–2), 86–95. DOI: [https://doi.org/10.1016/S0378-7753\(03\)00066-1](https://doi.org/10.1016/S0378-7753(03)00066-1)

- [242] S. B. Beale, S. V. Zhubrin, *Numer. Heat Transfer, Part B* **2005**, *47* (6), 573–591. DOI: <https://doi.org/10.1080/10407790590907930>
- [243] Z. He, H. Li, E. Birgersson, *Comput. Chem. Eng.* **2013**, *52*, 155–167. DOI: <https://doi.org/10.1016/j.compchemeng.2012.12.011>
- [244] T. T. Molla, K. Kwok, H. L. Frandsen, *Int. J. Hydrogen Energy* **2016**, *41* (15), 6433–6444. DOI: <https://doi.org/10.1016/j.ijhydene.2016.03.002>
- [245] Z. He, E. Birgersson, H. Li, *Int. J. Hydrogen Energy* **2014**, *39* (9), 4566–4575. DOI: <https://doi.org/10.1016/j.ijhydene.2013.12.203>
- [246] Z. He, E. Birgersson, H. Li, *Energy* **2014**, *70*, 478–492. DOI: <https://doi.org/10.1016/j.energy.2014.04.021>
- [247] E. Achenbach, *J. Power Sources* **1995**, *57* (1–2), 105–109. DOI: [https://doi.org/10.1016/0378-7753\(95\)02263-5](https://doi.org/10.1016/0378-7753(95)02263-5)
- [248] Y. Bae, S. Lee, K. J. Yoon, J.-H. Lee, J. Hong, *Energy Convers. Manage.* **2018**, *165*, 405–418. DOI: <https://doi.org/10.1016/j.enconman.2018.03.064>
- [249] Y. Bae, S. Lee, J. Hong, *Energy Convers. Manage.* **2019**, *201*, 112152. DOI: <https://doi.org/10.1016/j.enconman.2019.112152>
- [250] M. Nerat, *Energy* **2017**, *138*, 728–738. DOI: <https://doi.org/10.1016/j.energy.2017.07.133>
- [251] A. Al-Masri, M. Peksen, L. Blum, D. Stolten, *Appl. Energy* **2014**, *135*, 539–547. DOI: <https://doi.org/10.1016/j.apenergy.2014.08.052>
- [252] K. W. Eichhorn Colombo, V. V. Kharton, F. Berto, N. Paltrinieri, *Mater. Des. Process. Commun.* **2021**, *3* (5), e177. DOI: <https://doi.org/10.1002/mdp2.177>
- [253] A. Selimovic, M. Kemm, T. Torisson, M. Assadi, *J. Power Sources* **2005**, *145* (2), 463–469. DOI: <https://doi.org/10.1016/j.jpowsour.2004.11.073>
- [254] Z. Liang, J. Wang, Y. Wang, M. Ni, M. Li, *Energy Convers. Manage.* **2023**, *279*, 116759. DOI: <https://doi.org/10.1016/j.enconman.2023.116759>
- [255] M. Muramatsu, K. Yashiro, T. Kawada, K. Tarada, *Eng. Comput.* **2017**, *34* (6), 1956–1988. DOI: <https://doi.org/10.1108/EC-08-2016-0311>
- [256] P. Moçoteguy, A. Brisse, *Int. J. Hydrogen Energy* **2013**, *38* (36), 15887–15902. DOI: <https://doi.org/10.1016/j.ijhydene.2013.09.045>
- [257] Y. Wang, W. Li, L. Ma, W. Li, X. Liu, *J. Mater. Sci. Technol.* **2020**, *55*, 35–55. DOI: <https://doi.org/10.1016/j.jmst.2019.07.026>
- [258] S. Zarabi Golkhatmi, M. I. Asghar, P. D. Lund, *Renewable Sustainable Energy Rev.* **2022**, *161*, 112339. DOI: <https://doi.org/10.1016/j.rser.2022.112339>
- [259] J. Taubmann, X. Sun, C. Chatzichristodoulou, H. L. Frandsen, *ECS Trans.* **2023**, *111* (6), 955–964. DOI: <https://doi.org/10.1149/11106.0955ecst>
- [260] A. D. N. Kamkeng, M. Wang, *Chem. Eng. J.* **2022**, *429*, 132158. DOI: <https://doi.org/10.1016/j.cej.2021.132158>
- [261] A. Nakajo, P. Tanasini, S. Diethelm, D. Favrat, others, *J. Electrochem. Soc.* **2011**, *158* (9), B1102. DOI: <https://doi.org/10.1149/1.3596435>
- [262] M. Muramatsu, K. Terada, T. Kawada, K. Yashiro, K. Takahashi, S. Takase, *Comput. Mech.* **2015**, *56* (4), 653–676. DOI: <https://doi.org/10.1007/s00466-015-1193-7>
- [263] Y. Li, F. Grimm, J. Karl, *Fuel* **2023**, *343*, 127928. DOI: <https://doi.org/10.1016/j.fuel.2023.127928>
- [264] M. Navasa, H. L. Frandsen, T. L. Skafté, B. Sundén, C. Graves, *J. Power Sources* **2018**, *394*, 102–113. DOI: <https://doi.org/10.1016/j.jpowsour.2018.05.039>
- [265] M. Yan, M. Zeng, Q. Chen, Q. Wang, *Appl. Energy* **2012**, *97*, 754–762. DOI: <https://doi.org/10.1016/j.apenergy.2012.02.055>
- [266] G. Rinaldi, A. Nakajo, J. Van herle, P. Burdet, E. Oveisi, M. Cantoni, *ECS Trans.* **2017**, *78* (1), 3297–3307. DOI: <https://doi.org/10.1149/07801.3297ecst>
- [267] D. Klotz, A. Weber, E. Ivers-Tiffée, *Electrochimica Acta* **2017**, *227*, 110–126. DOI: <https://doi.org/10.1016/j.electacta.2016.12.148>
- [268] E. Ivers-Tiffée, A. Weber, *J. Ceram. Soc. Japan* **2017**, *125* (4), 193–201. DOI: <https://doi.org/10.2109/jcersj2.16267>
- [269] S. Dierickx, A. Weber, E. Ivers-Tiffée, *Electrochimica Acta* **2020**, *355*, 136764. DOI: <https://doi.org/10.1016/j.electacta.2020.136764>
- [270] F. Ravussin, J. Van herle, N. Autissier, M. Molinelli, D. Larrain, D. Favrat, *J. Eur. Ceram. Soc.* **2007**, *27* (2–3), 1035–1040. DOI: <https://doi.org/10.1016/j.jeurceramsoc.2006.05.089>
- [271] Z. Wuillemin, Y. Antonetti, C. Beetschen, O. Millioud, S. Ceschini, H. Madi, J. Van herle, *ECS Trans.* **2013**, *57* (1), 561–570. DOI: <https://doi.org/10.1149/05701.0561ecst>
- [272] E. Da Rosa Silva, G. Sassone, M. Prioux, M. Hubert, B. Morel, J. Laurencin, *J. Power Sources* **2023**, *556*, 232499. DOI: <https://doi.org/10.1016/j.jpowsour.2022.232499>

DOI: 10.1002/cite.202300137

High Temperature Solid Oxide Electrolysis – Technology and Modeling

Marius Mueller*, Markus Klinsmann, Ulrich Sauter, Jean-Claude Njodzefon, André Weber

Review Article: Solid oxide electrolyzers offer high efficiencies due to elevated operating temperatures. For the development of the technology experimental methods are limited. Physical modeling is therefore applied to investigate the complex and coupled physical processes occurring at various temporal and spatial scales within the cell. ■

